P-06-62

Oskarshamn site investigation

Determination of porosity and micro fracturing using the ^{14}C-PMMA technique in samples taken from Oskarshamn area

Laura Penttinen, Marja Siitari-Kauppi, Jussi Ikonen
Laboratory of Radiochemistry, Department of Chemistry,
University of Helsinki

November 2006

Svensk Kärnbränslehantering AB
Swedish Nuclear Fuel
and Waste Management Co
Box 5864
SE-102 40 Stockholm Sweden
Tel 08-459 84 00
+46 8 459 84 00
Fax 08-661 57 19
+46 8 661 57 19

ISSN 1651-4416
SKB P-06-62

Oskarshamn site investigation

Determination of porosity and micro fracturing using the ^{14}C-PMMA technique in samples taken from Oskarshamn area

Laura Penttinen, Marja Siitari-Kauppi, Jussi Ikonen
Laboratory of Radiochemistry, Department of Chemistry,
University of Helsinki

November 2006

Keywords: Rock porosity, Micro fracturing, ^{14}C-PMMA method, Image analyses.

Abstract

Porosity and micro fracturing were studied in the laboratory using samples taken from the Oskarshamn site investigation area. The purpose of the study was to determine the porosity pattern of 16 selected rock cores. The heterogeneities in porosities according to textural changes in rock minerals were determined.

The samples were studied by using the ^{14}C-PMMA method which gives the spatial distribution of porosity and micro fracturing in the samples. Comparable porosity measurements were performed using conventional water gravimetric measurements.

The rock samples varied from very tight and unaltered rock matrices having porosities about 0.1% to highly altered and weathered rocks which showed high PMMA porosities up to 20%. The average porosities of low porous rocks were in the range from 0.1% to 0.5%. The highest porosities were found in the matrices adjacent to the water bearing fracture zones which were altered and/or weathered. The fracture coating in one sample had four times higher porosity than the unaltered matrix. However, in some cases these zones were non porous indicating very low permeability.

Sammanfattning

Porositet och mikrosprickbildning har undersökts i prover tagna i Oskarshamns platsundersökningsområde. Syftet med undersökningen var att bestämma porositetsfördelningen i 16 utvalda bitar av borrkärna. Bestämningarna omfattade heterogeniteter i porositeten beroende på förändringar i mineralers textur.

Proverna undersöktes med ^{14}C-PMMA-metoden, vilken ger den rumsliga fördelningen av porositeten och mikrosprickbildningen i proverna. Jämförande porositetsmätningar gjordes med konventionell vattenmättnadsmetod.

Provbitarnas karaktär varierade från mycket tätt matrisberg med porositeter runt 0.1 % till kraftigt omvandlade och vittrade bitar med PMMA-porositeter upp till 20 %. Medelporositeten för den oomvandlade bergmatrisen var i storleksordningen mellan 0.1 % till 0.5 %. De högsta porositeterna uppmättes närmast intill vattenförande sprickzoner med omvandlat och/eller vittrat berg. I ett av proverna hade sprickfyllnadsmaterialet fyra gånger så hög porositet som den intilliggande, oomvandlade, bergmatrisen. I vissa fall hade dock även det omvandlade berget låg porositet, vilket indikerar låg permeabilitet.

Contents

1 Introduction

This report describes the study of the micro fracturing and porosity of rock cores taken from the boreholes KSH01–KSH03 and KLX02–KLX06 by using the ^{14}C-PMMA method (^{14}C-polymethylmethacrylate). The activity is related to the Site Investigation studies in Oskarshamn. The work is outlined in AP PS 400-03-041 and AP PS 400-03-093. The method description in detail is given by SKB MD 540.003 (Porositetsbestämning med PMMA). The PMMA method has been in continuous use in 1995–2004 for several applications needed for crystalline rock structure studies.

For the examination 16 cylindrical core samples were delivered to the Laboratory of Radiochemistry (HYRL) having diameters between 4.7 to 5.1 cm and different lengths from 5 cm to 20 cm. The rock types of the samples were granites, quartz monzodiorites, dioritoids, diorite-gabbro and variation of their alteration and weathering products. In addition a few samples were taken adjacent to the water bearing fracture zones.

In Table 1-1 controlling documents for performing this activity are listed. Both activity plan and method descriptions are SKB's internal controlling documents.

Table 1-1. Controlling documents for the performance of the activity.

Activity plan	**Number**	**Version**
Provtagning och analyser av borrkärna från KSH01 och KSH02 för bestämning av transportegenskaper	AP PS 400-03-041	1.0
Provtagning och analyser av borrkärna från KLX01-KLX04 för bestämning av transportegenskaper	AP PS 400-03-093	1.0
Method descriptions	**Number**	**Version**
Porositetsbestämning med PMMA	SKB MD 540.003	1.0

2 Objective and scope

The main focus of the work was to analyze the porosities and visualize the heterogeneous pore structure of rocks from the Oskarshamn site investigation area by using the ^{14}C-PMMA method. The method has been used previously to study the porosities and pore structures of different low porous media as well as to study the excavation damaged zones both in the Research Tunnel at Olkiluoto in Finland, the Äspö Hard Rock Laboratory in Sweden and Grimsel Underground Rock Laboratory in Switzerland. The experiences from the earlier analysis have shown that the technique can be applied effectively to study the spatial distribution of porosity in the low porous media. The porosity profiles adjacent to water bearing fracture zones can also be studied.

The objective of the activity is to provide visualisation and quantitative results on:

- interconnected porosities of rock samples,
- porosity profiles of altered zones next to water conducting, or presumptive water conducting, fractures,
- micro fracturing of rock samples.

3 Materials

The sixteen samples were received at HYRL in two batches. An internal HYRL code was given (O1–O13) and they were photographed. Appendices 1–16 present the photo images of each sample before any operation. The lengths and widths of the samples and their codes are presented in Table 3-1. Samples O1–O5 and O13–O15 were cut into two or three pieces with a diamond saw to have separate pieces for PMMA analysis and for water gravimetry measurements (see partition diagrams in Appendices 1–6 and 13–15). The other samples were impregnated without cutting. The sawing scheme for autoradiography after PMMA impregnation is shown in Appendices 1–16. The diamond saw used in the experiment was of the Eurocoup-Masondry type. The thickness of the blade was 1.8 mm and ∅350 mm. The speed of rotation was 2,800 rpm and the loss of rock matrix 2.1 mm. Appendix 17 presents the initial data provided by SKB (Eva Gustavsson, Geosigma AB) containing a short description of sample types and sampling depths.

Table 3-1. Sample codes, section details, diameters, porosity results from SKB, lengths before sawing, lengths for sawn samples used in PMMA and water gravimetry (H_2O) analysis.

Code HYRL	Code SKB	Secup (m)	Seclow (m)	Diameter (mm)	SKB porosity (%)	Length before sawing (cm)*	PMMA samples (cm)**	H2O samples (cm)*
O1	KSH01	714.89	715.04	50	0.15	15	2.8	1.9
O2	KSH02	600.31	600.41	50	0.18	10	1.8	3.4
O3	KLX02	216.56	216.66	47	0.3	10	3.4	1.7
O4	KLX02	683.43	683.53	47	0.08	10	2.0	2.0
O5	KLX06	112.70	112.92	50	–	20	3.0 7.0 8.0	2.0
O6	KLX06	409.69	409.83	51	–	11 / 15	11 / 15	–
O7	KSH02	398.93	399.05	50	–	8.7 / 14	8.7 / 14	–
O8	KSH02	743.00	743.05	50	–	4.1 / 5	4.1 /5	–
O9	KLX02	385.50	385.60	40	–	10	10	–
O10	KLX03	725.47	725.72	50	–	14 / 19.5	9.5 / 11	–
O11	KLX04	897.07	897.17	50	–	9 / 11.5	9 / 11.5	–
O12	KLX04	941.81	941.91	50	–	7 / 10.1	7 / 10.1	–
O13	KLX05	363.91	364.02	50	–	11	4.1	2.1
O14	KLX05	722.39	722.49	50	–	10	3.7	1.6
O15	KLX06	318.90	319.00	50	–	9 / 10.1	4.2 / 5.2	1.9
O16	KSH02	288.86	289.08	50	–	21 / 23	11.7	–

* lengths as average,

** lengths are taken from the shortest and longest locations.

4 Methods

4.1 Water gravimetry

Water gravimetry was performed for rock samples O1–O5 and O13–O15 to roughly evaluate the impregnation time needed for thorough intrusion of impregnant. Rock samples O6–O12 and O16 were analysed as whole and cutting for water gravimetry subsamples was not required. The water porosity determined relative to time gives us the rate of intrusion indicating roughly how easily the interconnected pore network was filled with water and consequently also with PMMA. The modified water gravimetry method used here was produced during the development of the PMMA technique and is not a standard method.

The samples for water gravimetry analysis were desiccated in 105°C degrees for 7 days. After cooling, they were emerged into milliQ water in separate tubs and weighed every hour during the first day to monitor the impregnation of water inside the rock. The experiment was carried out for 38–42 days, the results for the H_2O samples can be found in Figures 4-1 and 4-2. The uncertainty is about 10%. After approximately two weeks of impregnation the maximum porosity value was reached in these samples. The sample O5 having a porosity value of 0.6% after two weeks of impregnation showed an anomalous increase after four weeks of impregnation for an unknown reason.

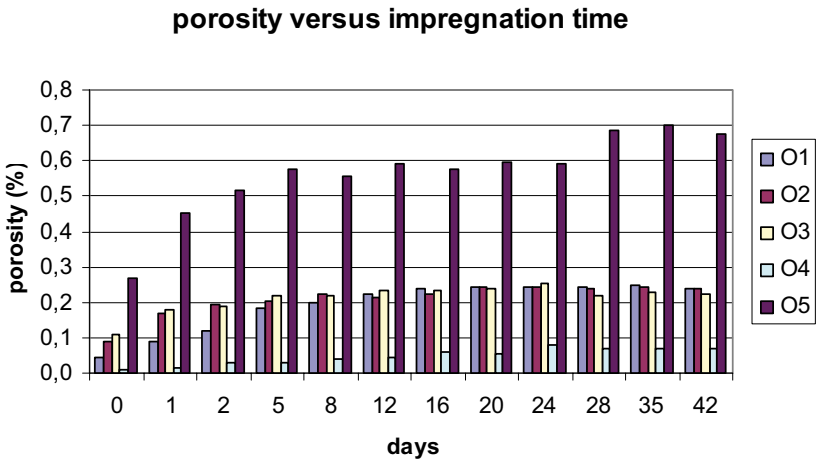

Figure 4-1. *Water gravimetry results for samples O1, O2, O3, O4 and O5.*

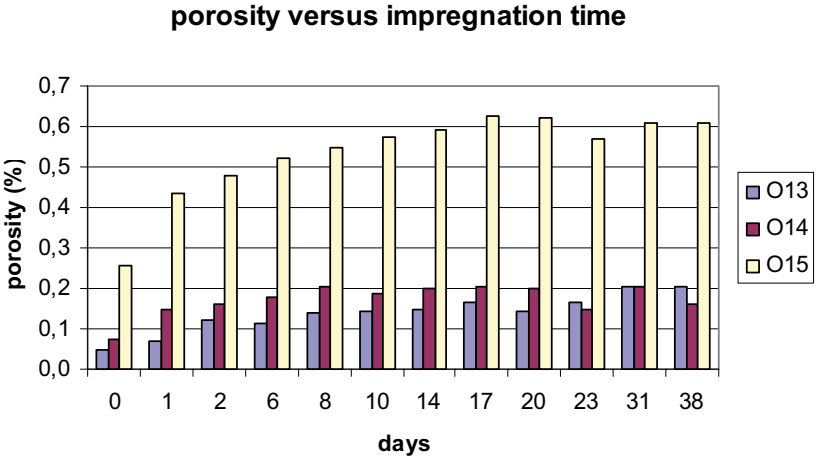

Figure 4-2. *Water gravimetry results for samples O13, O14 and O15.*

4.2 ^{14}C-PMMA method

The ^{14}C-PMMA method involves the impregnation of centimetre-scale rock cores with ^{14}C labelled methylmethacrylate (^{14}C-MMA) in a vacuum, irradiation polymerisation, autoradiography and optical densitometry using digital image-processing techniques /1–6/. Impregnation with ^{14}C-MMA, a labelled low-molecular-weight and low-viscosity monomer which wets the silicate surfaces well and which can be fixed by polymerisation, provides information about the accessible pore space in crystalline rock that cannot be obtained using other methods. The method has been described in the report "Use of the ^{14}C-PMMA and He-gas methods to characterize excavation disturbance in crystalline rock" by Autio /7/.

Total PMMA porosity, i.e connected porosity, is calculated by using 2D autoradiographs of the sawn rock surfaces. The geometry of porous regions is then visualised. The conditions for applying this method are: (i) a known local bulk density; (ii) the presence of only two phases, i.e. mineral and PMMA; and (iii) a homogeneous distribution of pores and minerals below the lateral resolution limit of autoradiography.

4.2.1 Properties of ^{14}C-MMA tracer

Methylmethacrylate (MMA) is a monomer with a viscosity 0.00584 Pas (20°C) /8/ that is significantly lower than the viscosity of water 0.00895 Pas (25°C) /9/. Table 4-1 lists the viscosities of the epoxy and acrylic resins used in Swiss experiments /10/ as well as the viscosity of MMA and water. All the resins are widely used for matrix characterization purposes. Because its contact angle on silicate surfaces is low, impregnation of bulk rock specimens by MMA is rapid by capillary forces and dependent on the existing pore apertures. The MMA molecule is small (molecular weight 100.1), it has non-electrolytic properties and only low polarity, the polarity of the ester being considerably lower than that of water. In the rock matrix MMA behaves like a non-sorbing tracer. The low β energy of the carbon-14 isotope, a maximum of 155 keV, is convenient for autoradiography measurements.

The monomer from which the dilutions with inactive MMA (MMA for analyses, Merck) were done was ^{14}C-labelled MMA with a specific activity of 2–5 mCi/g and a radiochemical purity of > 95%. In this study, the dilution of the tracer varied between 37 kBq/ml (1 μCi/ml) and 1,110 kBq/ml (30 μCi/ml). The calibration sources activities ranged from 462 Bq/ml (12.5 nCi/ml) to 185,000 Bq/ml (5 μCi/ml).

4.2.2 Drying, impregnation and irradiation of samples

Samples were vacuum-dried in aluminium chambers for 3–26 days at a maximum temperature of 105°C and then cooled to 18°C. Impregnation with ^{14}C-MMA was carried out by placing the tracer in a 50 ml reservoir and transferring it under vacuum into the impregnation chamber. Slow transfer of the monomer ensures degassing and infiltration of the sample without vapour.

Table 4-1. Viscosities of MMA used in this work, water, epoxy resin /10/ and acrylic resin /10/ used in Swiss experiments.

resin	viscosity Pa s
MMA	0.00584 (20°C)
water	0.00895 (25°C)
acrylic resin	≈0.03 (5°C), < 0.01(20°C)
epoxy resin	0.15 (13°C), 0.1 (23°C)

Impregnation time varied between 13 and 30 days. After impregnation, samples were irradiated with gamma rays from a Co-60 source to polymerise the monomer in the rock matrix; the dose required was 70 kGy (7 Mrad). Samples were irradiated in glass or polyethylene vials under water and ^{14}C-MMA emulsion. In addition, a few highly or moderately porous samples had to be irradiated under active tracer to avoid any outdiffusion of ^{14}C-MMA from the rock sample during irradiation which took from 5 to 7 days. Appendix 18 lists the experimental procedure for the studied samples.

4.2.3 Autoradiography

Irradiation of rocks with Co-60 causes strong thermoluminescence in K-feldspar and other major rock-forming minerals which exposes autoradiography film. To avoid this effect, the thermoluminescence was released by heating the impregnated and irradiated samples to 120°C for a period of 3 hours prior to sawing. Mylar foil with an aluminium coating was used to shield the film from the rest of emissions.

After heating, the samples were sawn into pieces as shown in the partition diagrams in Appendices 1–16. The sawn rock surfaces were exposed on Kodak BioMax MR film, a high-performance autoradiography film for ^{14}C and other low-energy β-emitting nuclides. The nominal resolution of the β film is a few μm. The final spatial resolution achieved depends on the roughness of the sawn surface, the space between the rock and autoradiography film and the range of the 155 keV beta particles in the rock matrix.

With the level of tracer activity and the type of autoradiography film employed, the exposure times for samples ranged from 4 to 25 days. While the short exposure times are convenient for the quantitative determination of porosity, the longer exposure times are better for the qualitative determination of microfracturing. The employed exposure times are listed in Appendix 18.

Sensitivity

The detection system of autoradiography refers to nuclear emulsion of the autoradiography film and the measurement of the blackening of the film by digitizing the intensities (grey levels) of the film. Since the response of the image source and the amplifier of the digital image analysator are linear, the digitised grey levels of the film can be treated as intensities and converted to optical densities, which are defined as decadic logarithm of the intensity ratio of background to sample sub-domains, thus the blackening is related to silver grain density according to Lambert & Beer's law and is concentration proportional. The linearity of the film autoradiography is much lower than the modern FLA scanner technique, which is described in Chapter 4.3.

The sensitivity of the autoradiography film is declared as a function of exposure time, the activity of the radiation source per square area and the blackening of the autoradiography film. Figure 4-3 shows the effect of exposure time on the optical densities of the ^{14}C-PMMA calibration sources, which are dilutions of the used tracer. An example of an autoradiograph of 5 days exposed calibration sources is included. The nonlinear response of the autoradiography method at high concentrations can be seen and the saturation of the autoradiography film at optical density values of around 1.8 is detected. For one day exposure, linearity is kept through the activity range. For longer exposure times, curves are composed of two slopes that underscores the nonlinear response of the nuclear emulsion at high concentrations.

Resolution

The radiographic image of a point is not a point, but it is made up from developed silverhalogenide crystals located at different distances from the source. Figure 4-4 show a backscattered electron image of the PMMA impregnated rock sample and the corresponding autoradiograph digitized by CCD camera (Hamamatsu). The figure illustrate the spatial resolution of autoradiography method. The porous minerals form even grey areas on the autoradiograph.

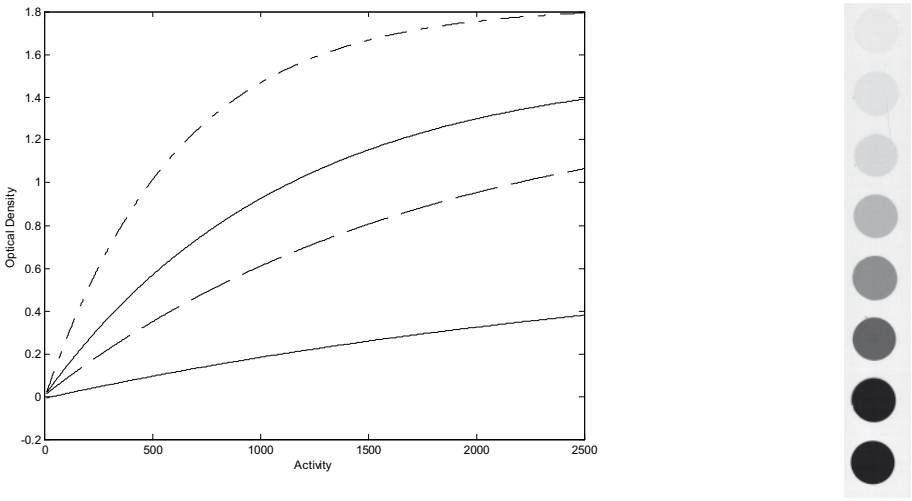

a *b*

Figure 4-3. *a) Optical densities of ^{14}C-PMMA calibration sources of different exposure times:1, 2, 5 and 15 days exposed on Kodak Biomax MR autoradiography film – scanned with Ricoh FS2 flatbed scanner using 300 dpi resolution. b) An autoradiograph of the calibration sources exposed 5 days.*

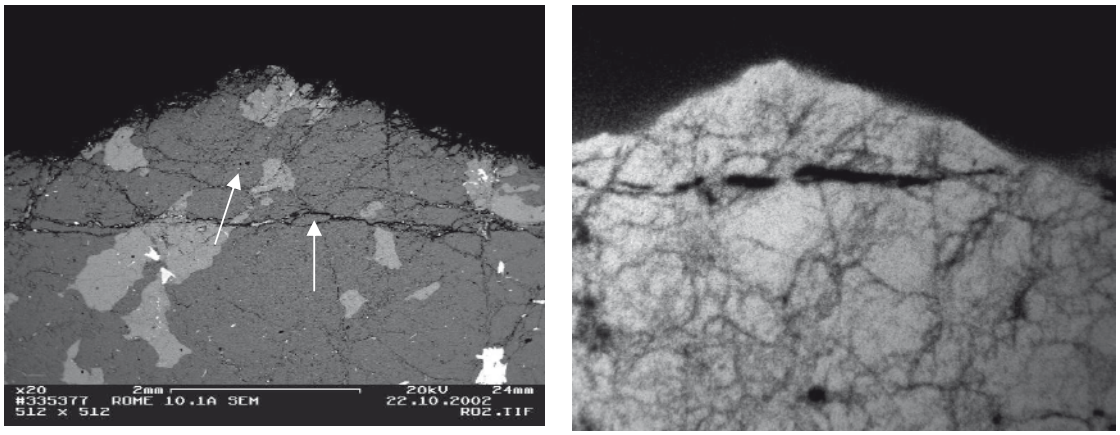

a *b*

Figure 4-4. *Backscattered electron image (a) and corresponding autoradiograph (b) of PMMA impregnated rock sample illustrating resolution characteristics of the method.*

The energy of the used radioactive nuclide has high impact on the resolution. It influences both the range in the rock as well as the absorption of the beta particles on the autoradiography film emulsion layer. Other important factors for the resolution are the distance between the autoradiography film and the rock source and the quality of the rock surfaces.

4.2.4 Digital image analysis of ^{14}C-PMMA autoradiographs

Interpretation of the results is based on digital image analysis of the autoradiograph. Digital image analysis started by dividing the autoradiograph into area units called pixels. The rock surfaces and the film autoradiographs were digitized with Canon 9900 table scanner using 1,200 dpi resolution. In this study, the 600 dpi resolution is used in the quantitative analysis. Essentially, all the intensities of the sub-domains were converted into corresponding optical densities, and these were in turn converted into levels of activity with the help of the calibration curves measured for each exposure. Finally, the levels of activity were converted into their corresponding porosities. In principle, the interpretation is based on studying the abundance

of tracer in each sub-domain. Reference /1/ contain the basic calculations related to porosity determination. The software program Mankeli for quantitative porosity measurement was used in this study, implemented using the Matlab Image Processing Toolbox.

Calculation of porosity

Intensity and optical density

Since the response of the image source (a flatbed scanner) and the amplifier of the digital image analyser are linear, the digitised grey levels of the film can be treated as intensities. Optical densities, which according to Lambert & Beer's law are proportional to concentration, are derived from the intensities:

$$D = -\log\left(\frac{I}{I_0}\right) \qquad 4\text{-}1$$

where D is the optical density, I_0 is the intensity of the background and I is the intensity of the sample. It can be seen that as the intensity decreases, the optical density increases.

Activity and optical density

A conversion function is required to relate the measured optical densities to the corresponding levels of activity. ^{14}C-PMMA standards (tracer diluted with inactive MMA) having specific activities between 462 and 185,000 Bq/ml were used to establish the calibration function. The construction of the calibration curves which enable the quantitative measurement of the autoradiograph obtained by the PMMA method is conducted by an iterative calculation of three parameters (a,k,c). For a given exposure time the mathematical function describing the nonlinear behaviour of the local activity versus optical density of the film has the principle form:

$$D = a(1 - e^{-kA}) + c \qquad 4\text{-}2$$

where D is the optical density and A is the specific activity. The equation is written in the form:

$$\ln(A_b - D) = -kA + C \qquad 4\text{-}3$$

where the parameters A_b= a+c = D_{max}, k and C= ln(a) = D_0 are found iteratively by the least squares method (first the value of A is iterated to give the best correlation with the data points and then k and C are calculated) and the activity in the rock sample is calculated from the measured optical density. Solving A from above equation gives:

$$A = \frac{\ln(D_{\max} - D) - D_0}{-k} \qquad 4\text{-}4$$

Porosity

The local porosity ε of the sample was simply obtained from the abundance of the tracer (assuming that the concentration of tracer in the PMMA is constant, the higher the abundance of the tracer, the higher the local porosity):

$$\varepsilon = \beta(A / A_0) * 100\% \qquad 4\text{-}5$$

where A_0 is the specific activity of the tracer used to impregnate the rock matrix, and β is the β-absorption correction factor. The absorption of β radiation in a substance depends on the density of the substance in a roughly linear fashion. The factor β can therefore be approximated from:

$$\beta = \rho_s / \rho_0 \qquad 4\text{-}6$$

where ρ_s is the density of the sample and ρ_0 is the density of pure PMMA (1.18 g/cm^3). In this interpretation, the sample is assumed to consist of rock material and pores (containing PMMA). ρ_s can therefore be expressed as:

$$\rho_s = \varepsilon\rho_0 + (1 - \varepsilon)\,\rho_r \qquad 4\text{-}7$$

where ρ_r is the density of the mineral grains. In bulk measurements the average density of the rock sample is used instead of mineral density. Using Equations 4-6 and 4-7 in Equation 4-5, the porosity and the activity relationship can be solved:

$$\varepsilon = \frac{\dfrac{\rho_r}{\rho_0}}{1 + \left(\dfrac{\rho_r}{\rho_0} - 1\right)\dfrac{A}{A_0}}\,\frac{A}{A_0} \qquad 4\text{-}8$$

where A is the specific activity of individual pixel and A_0 is the specific activity of the tracer. The porosity of each individual pixel n from the autoradiogram is calculated according to Equations 4-4 and 4-8. The porosity histogram provides the relative frequency of regions of different individual porosities. The total PMMA porosity is obtained from the porosity distribution by taking a weighted average:

$$\varepsilon_{tot} = \frac{\sum_n Area_n \varepsilon_n}{\sum_n Area_n} \qquad 4\text{-}9$$

where $Area_n$ is the area of pixel n, and ε_n is the local porosity of pixel n.

The amount of tracer in the sample, and the volumetric porosity, can therefore be derived from the blackening of the film caused by the radiation emitted from the plane surface of the rock section. Figure 4-5 shows an example of the autoradiograph and the porosity distribution of Sample O2. If the pore sizes are well below the resolution of the autoradiography, the major fraction of the beta radiation emitted is attenuated by silicate. The tracer can thus be considered to be diluted by silicate. For the ^{14}C-PMMA method to be used, the bulk density must be known, there must be only two phases (i.e. mineral and PMMA), and the pores and minerals must be homogeneously distributed below the lateral resolution limit of the autoradiography.

Porosity profiles were measured from the autoradiograph if the sample was taken adjacent to the water bearing fracture and the porosity pattern showed any changes according to the distance from the surface. Figure 4-6 shows a profile measurement example measured from the autoradiograph of Sample O12.

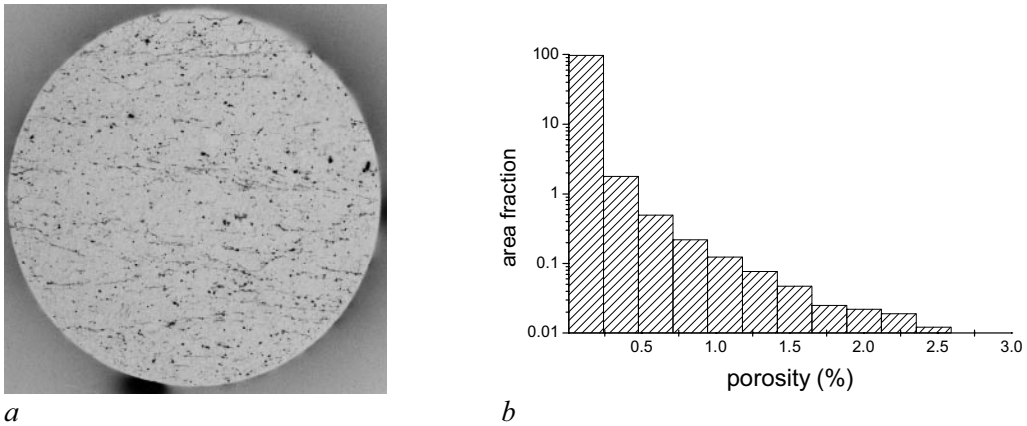

a *b*

Figure 4-5. *a) Autoradiograph of Sample O2 and b) corresponding porosity histogram. Total PMMA porosity of 0.13% was determined. Sample diameter is 51 mm.*

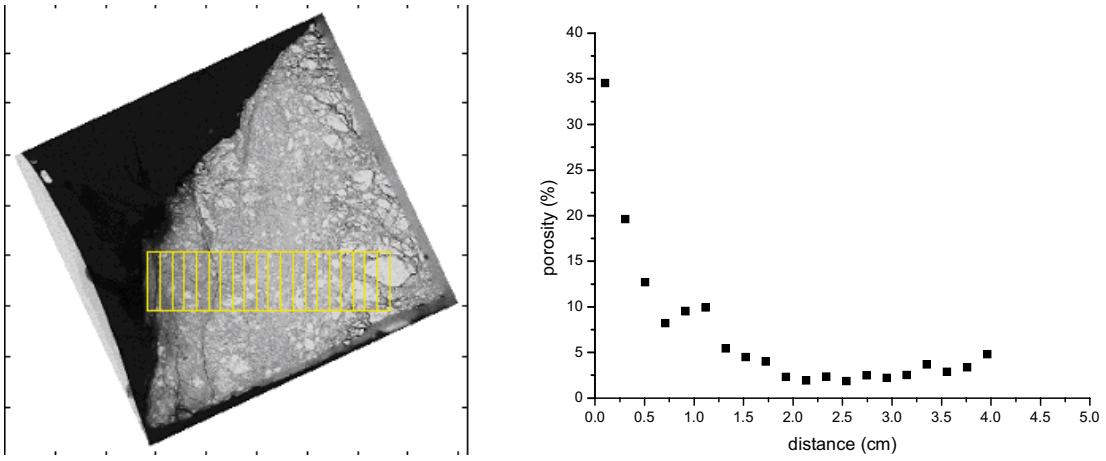

a *b*

Figure 4-6. *a) Autoradiograph of Sample O12. Fracture surface is on the left of this image. Sample width is 4 cm. b) Porosity profile measured from the autoradiograph.*

4.3 Digital autoradiography with FLA-5100

The new FujiFilm FLA-5100 imaging system allows imaging of fluorescent and radioisotopic samples. Imaging Plates are flexible image sensors in which bunches of very small crystals of photo-stimulable phosphor of barium fluorobromide containing a trace amount of bivalent europium as a luminescence center, formulated as BaFBr:Eu2+, are uniformly coated on a polyester support film. Exposure of samples on an imaging plate is similar to that of photo-film but it can be reused after erasing the latent image from the plate with uniform white light.

The area of linearity achieved with the FLA-5100 scanner is five orders of magnitude, when the linear area in film autoradiograhy is only two orders of magnitude. The IPs are 50–100 times more sensitive than autoradiography films. This allows shorter exposure times and a better separation power when using samples with high energy nuclides.

This study provided an excellent opportunity for HYRL to compare the two different imaging methods: film autoradiography and digital autoradiography. All the samples have been imaged with both methods, but the quantitative porosity analysis has been done from film autoradiographs. The images achieved with the FLA-5100 scanner are presented in this report as colour images in next chapter.

5 Results of PMMA analyses

5.1 Sample O1 (KSH01)

The photograph taken of sample O1, before any operation, and the partition diagram are presented in Appendix 1. A photo image of the analysed rock surface is presented below in Figure 5-1a and the corresponding film and digital autoradiographs are shown in Figures 5-1b and 5-1c, respectively. The exposure time on the film autoradiograph has been 21 days and on the digital autoradiograph 3 days.

The PMMA porosity of the O1 sample is 0.05%. Figure 5-2 shows the porosity histogram for O1 achieved with the PMMA method. The rock sample has been fully impregnated, porous veins transect the rock core. These porous veins cannot be separated easily from the photo image of the rock surface. An intra granular porosity pattern is found, no grain boundaries are dominating this porosity pattern visualised by PMMA method. With water gravimetry the porosity for sample O1 was 0.2%.

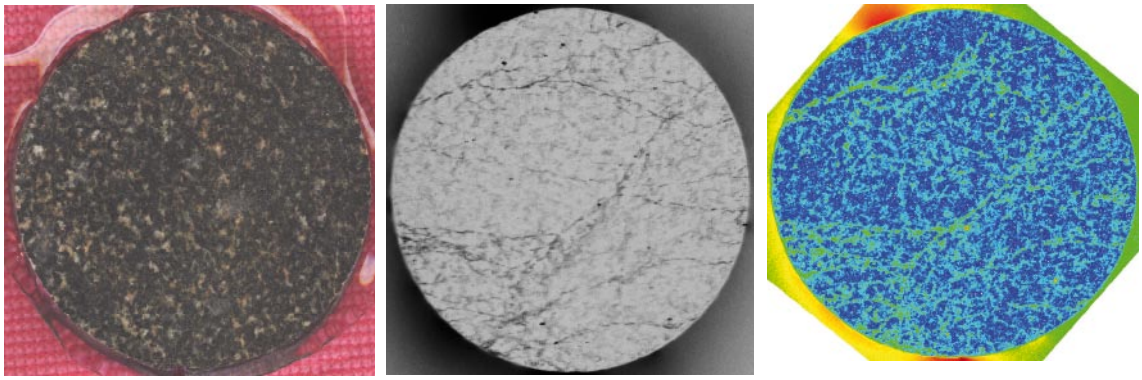

a *b* *c*

Figure 5-1. *a) the analysed rock surface of sample O1, b) its corresponding film autoradiograph and c) its corresponding digital autoradiograph.*

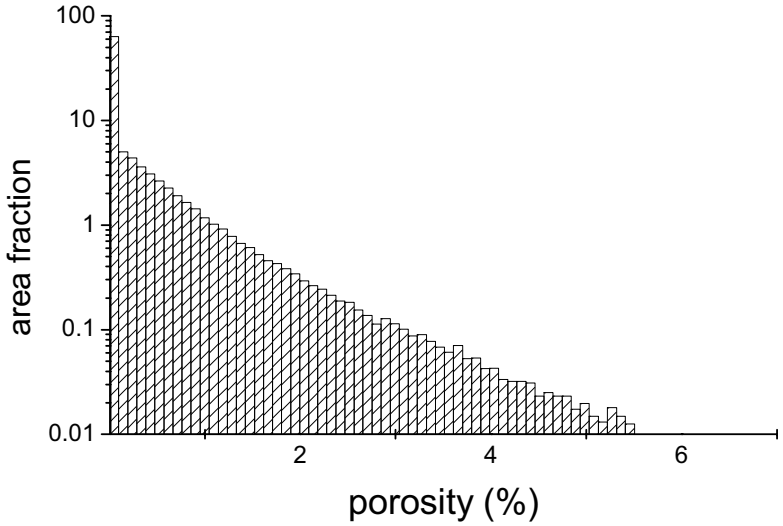

Figure 5-2. *Porosity histogram of sample O1. A total PMMA porosity of 0.05% was determined.*

5.2 Sample O2 (KSH02)

The photograph taken of sample O2, before any operation, and the partition diagram are presented in Appendix 2. A photo image of the analysed rock surface is presented below in Figure 5-3a and the corresponding film and digital autoradiographs are shown in Figures 5-3b and 5-3c, respectively. The exposure time on the film autoradiograph has been 21 days and on the digital autoradiograph 3 days.

The PMMA porosity for the O2 sample is 0.13%. Figure 5-4 shows the porosity histogram for O2 achieved with the PMMA method. The rock sample has been fully impregnated, grain boundary porosity dominates. Intra granular porosity is found in a few mineral phases which cause slight foliation in the porosity pattern. With water gravimetry the porosity for sample O2 was 0.2%. Figure 5-5 shows porosities of over 0.2% emphasized on the autoradiograph in red.

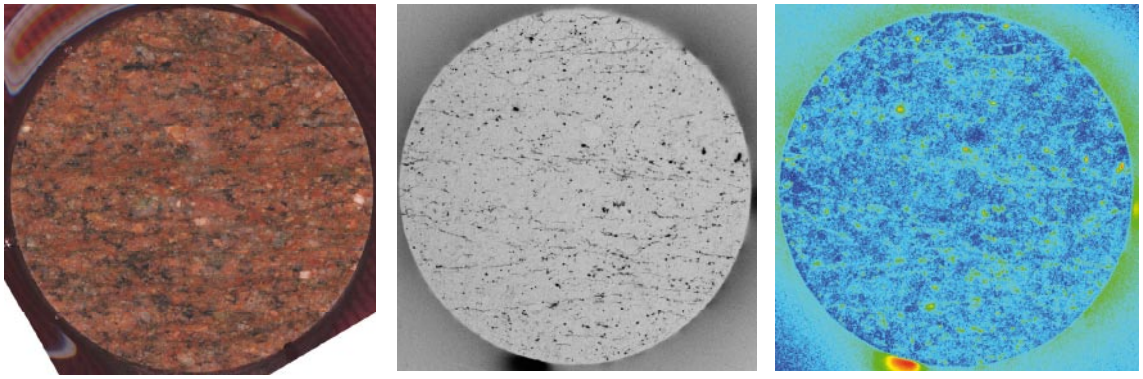

a *b* *c*

Figure 5-3. *a) the analysed rock surface of sample O2, b) its corresponding film autoradiograph and c) its corresponding digital autoradiograph.*

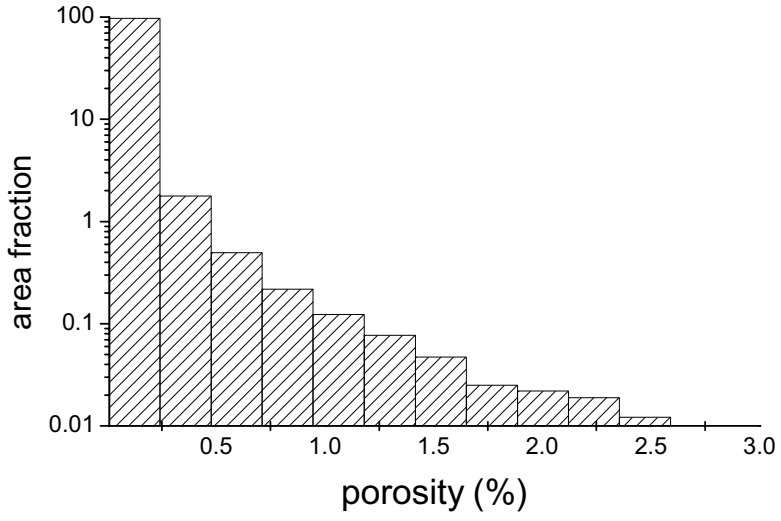

Figure 5-4. *Porosity histogram of sample O2. A total PMMA porosity of about 0.13% was determined.*

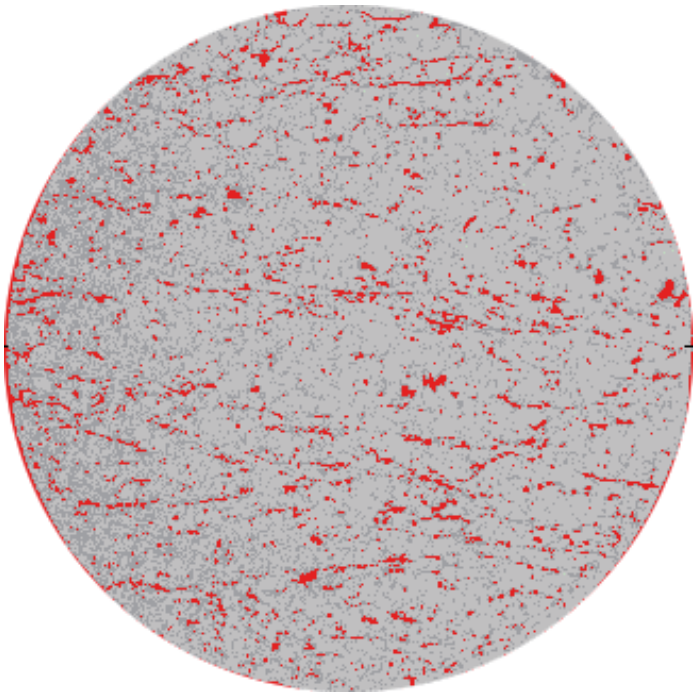

Figure 5-5. *Autoradiograph of sample O2 with porosities of over 0.2% shown in red.*

5.3 Sample O3 (KLX02)

The photograph taken of sample O3, before any operation, and the partition diagram are presented in Appendix 3. A photo image of the analysed rock surface after impregnation and sawing is presented below in Figure 5-6a and the corresponding film and digital autoradiographs are shown in Figures 5-6b and 5-6c, respectively. The exposure time on the film autoradiograph has been 21 days and on the digital autoradiograph 3 days.

The PMMA porosity for the O3 sample is 0.12%. Figure 5-7 shows the porosity histogram for O3 achieved with the PMMA method. The rock sample has been fully impregnated, grain boundary porosity was found, however a few porous patches congruent with mafic minerals are present. The porosity pattern shows slight foliation. With water gravimetry the porosity for sample O3 was 0.2%. Figure 5-8 shows porosities of over 0.2% emphasized on the autoradiograph in red.

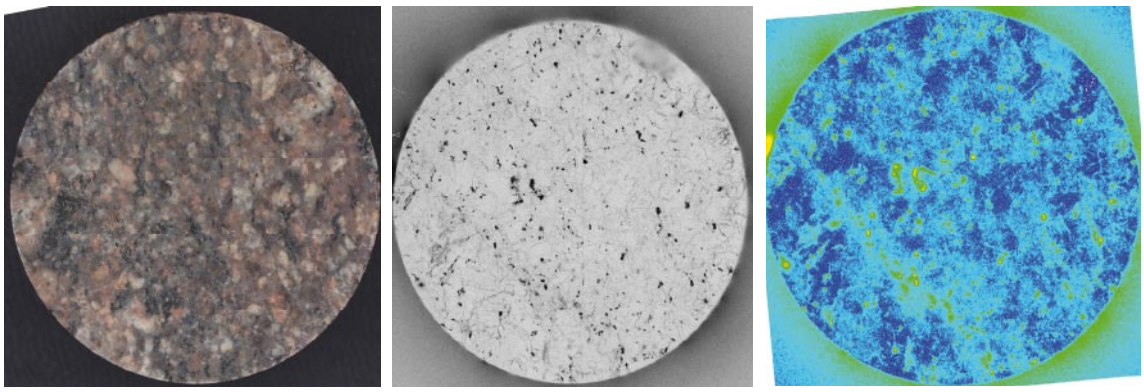

a *b* *c*

Figure 5-6. *a) the analysed rock surface of sample O3, b) its corresponding film autoradiograph and c) its corresponding digital autoradiograph.*

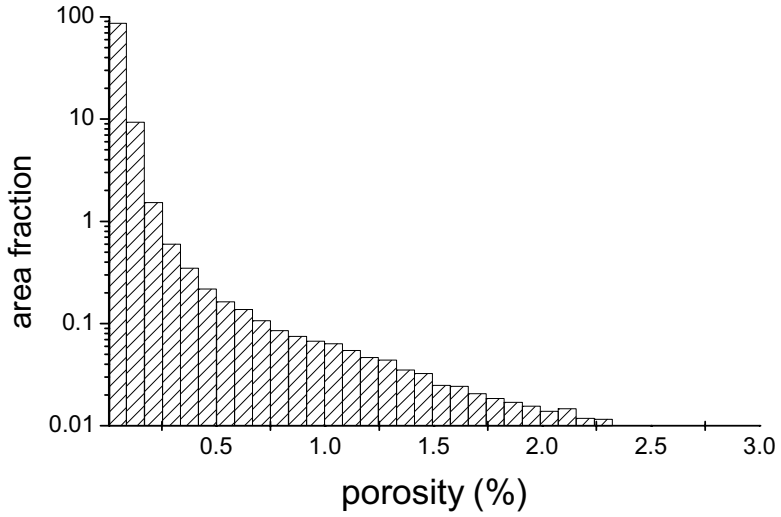

Figure 5-7. *Porosity histogram of sample O3. A total PMMA porosity 0.12% was determined.*

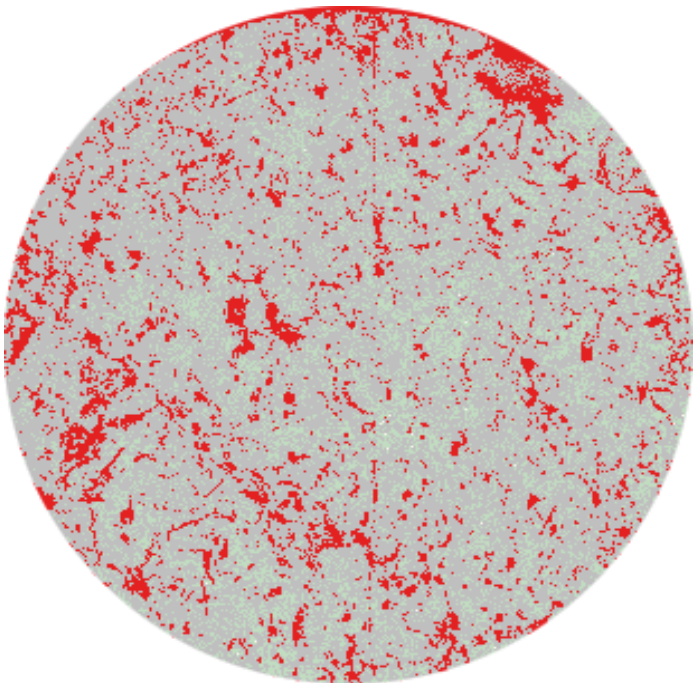

Figure 5-8. *Autoradiograph of sample O3 with porosities of over 0.2% shown in red.*

5.4 Sample O4 (KLX02)

The photograph taken of sample O4, before any operation, and the partition diagram are presented in Appendix 4. A photo image of the analysed rock surface after impregnation and sawing is presented below in Figure 5-9a and the corresponding film autoradiograph is shown in Figure 5-9b. The exposure time on the film autoradiograph has been 28 days and on the digital autoradiograph 3 days.

Figure 5-9 shows clearly that the sample O4 is nonporous with the PMMA-method. The MMA has not intruded into the rock indicating tight and very low permeable matrix. With water gravimetry the porosity for sample O4 H_2O was 0.03%.

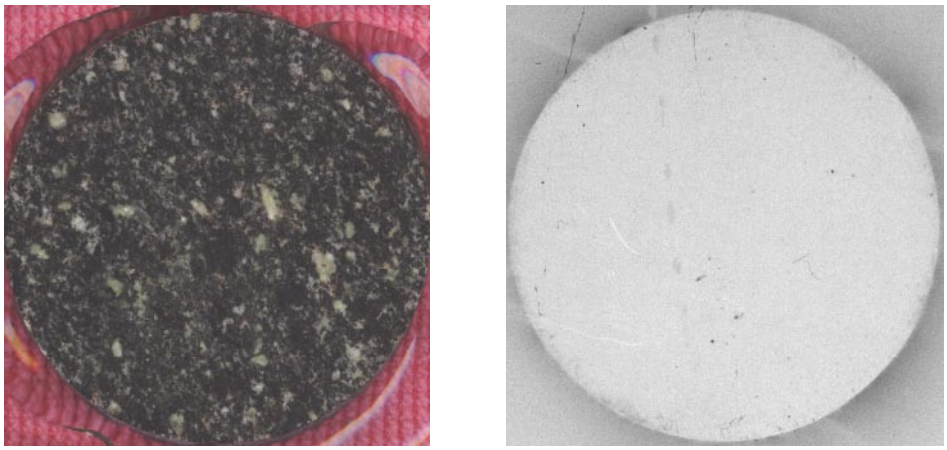

a *b*

Figure 5-9. *a) the analysed rock surface of sample O4 and b) its corresponding film autoradiograph.*

5.5 Sample O5 (KLX06)

The photograph taken of sample O5, before any operation, and the partition diagram are presented in Appendix 5. The sample was already in two pieces, the longer piece was sawn into three pieces, one for water gravimetry analysis and two for PMMA analysis. The shorter piece was impregnated whole. The sample O5A was taken at a depth of 17 cm and the sample O5B 8 cm from the fracture surface. The sample O5C contained the fracture surface representing a profile to a depth of 8 cm from the fracture surface. The photo images of the analysed rock surfaces after impregnation and sawing are presented below in Figures 5-10a, 5-11a and 5-12a, the corresponding film and digital autoradiographs for sample O5A are shown in Figures 5-10b and 5-10c, for sample O5B in Figures 5-11b and 5-11c, and for sample O5C in Figures 5-12b and 5-12c, respectively. For all samples the exposure time on the film autoradiograph was 21 days and on the digital autoradiograph 3 days.

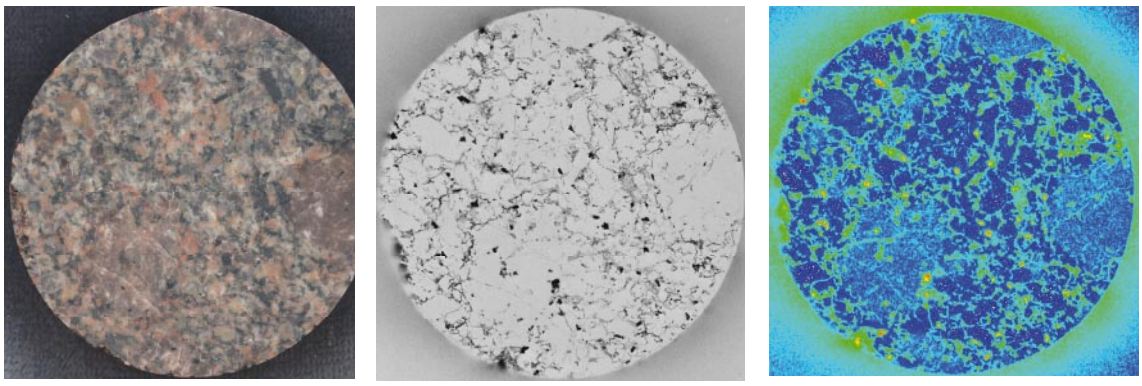

a *b* *c*

Figure 5-10. *a) the analysed rock surface of sample O5A, b) its corresponding film autoradiograph and c) its corresponding digital autoradiograph.*

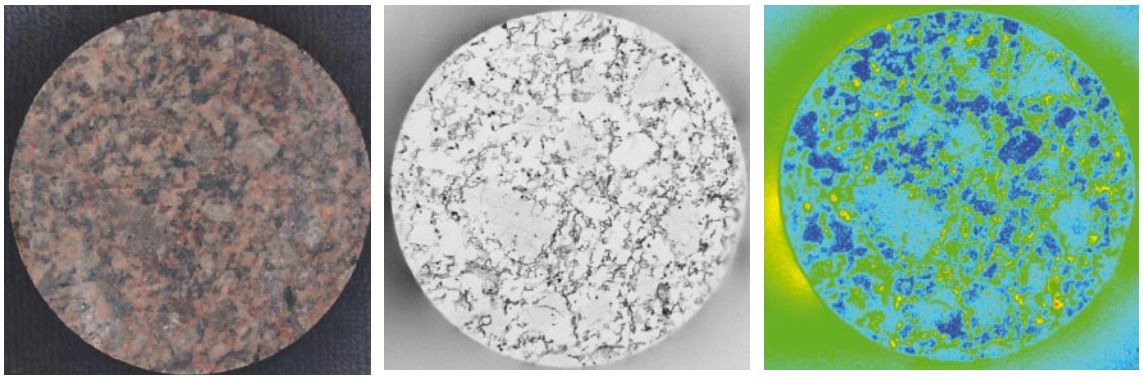

a *b* *c*

Figure 5-11. *a) the analysed rock surface of sample O5B, b) its corresponding film autoradiograph and c) its corresponding digital autoradiograph.*

a

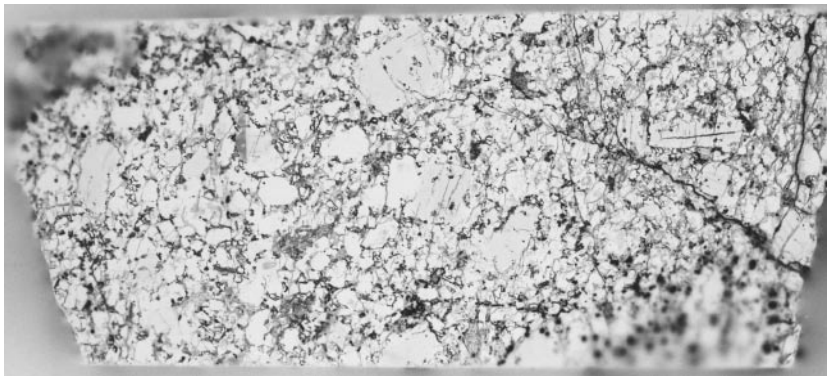

b

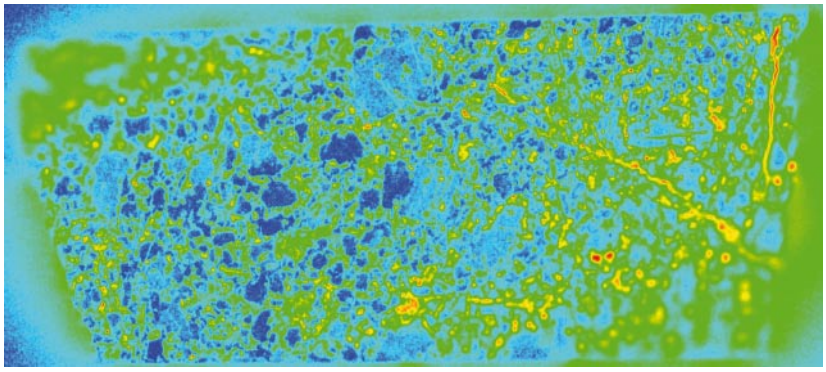

c

Figure 5-12. *a) the analysed rock surface sample of sample O5C, b) its corresponding film autoradiograph and c) its corresponding digital autoradiograph. The fracture surface is on the right hand side in the images.*

The PMMA porosity for the sample O5C was 0.8%. No clear porosity profile could be found, i.e. decreasing porosity from the fracture surface to depths into the non altered matrix. However, a few fractures existing parallel and perpendicular to the fracture surface in this sample was found. The PMMA porosity for the sample O5B was 0.7%, and for the sample O5A, 0.4%. The grain boundary porosity dominates in sample O5A. Porosity pattern is strongly heterogeneous in all samples. Figure 5-13 shows the porosity histogram for O5C achieved with the PMMA method. The sample has been fully impregnated, intra granular porosity is found in mafic mineral grains and in some feldspar grains. Quartz grains are non porous by the PMMA method, but a few tiny micro fissures transect these grains. Not exact mineral grain boundary porosity is found in O5B and O5C, but porous minerals form connective migration pathways in 2D. With water gravimetry the porosity for sample O5 was 0.6%.

5.6 Sample O6 (KLX06)

The photograph taken of sample O6, before any operation, and the partition diagram are presented in Appendix 6. After impregnation the sample was sawn into two pieces. The photo images of the analysed rock surfaces after impregnation and sawing for sample O6A and O6B are presented below in Figures 5-14a and 5-15a, the corresponding film and digital autoradiographs for sample O6A are shown in Figures 5-14b and 5-14c, and for O6B in Figures 5-15b and 5-15c, respectively. The exposure time on the film autoradiographs was 21 days and on the digital autoradiographs 3 days.

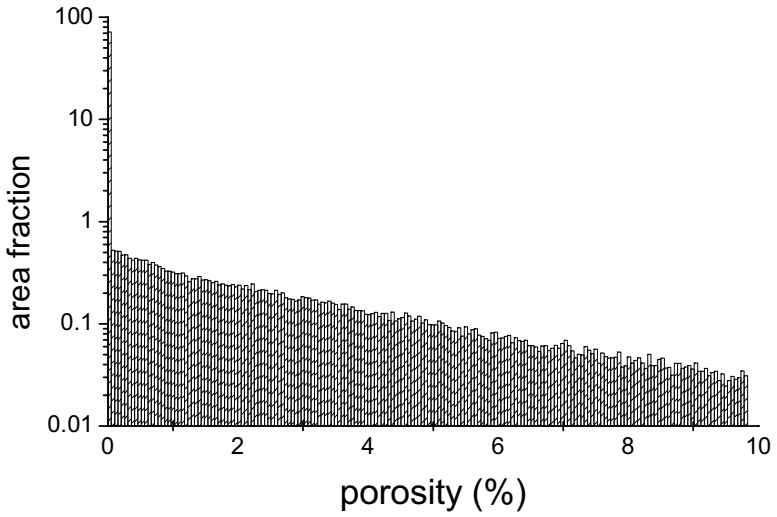

Figure 5-13. *Porosity histogram of sample O5C. A total PMMA porosity of about 0.8% was determined.*

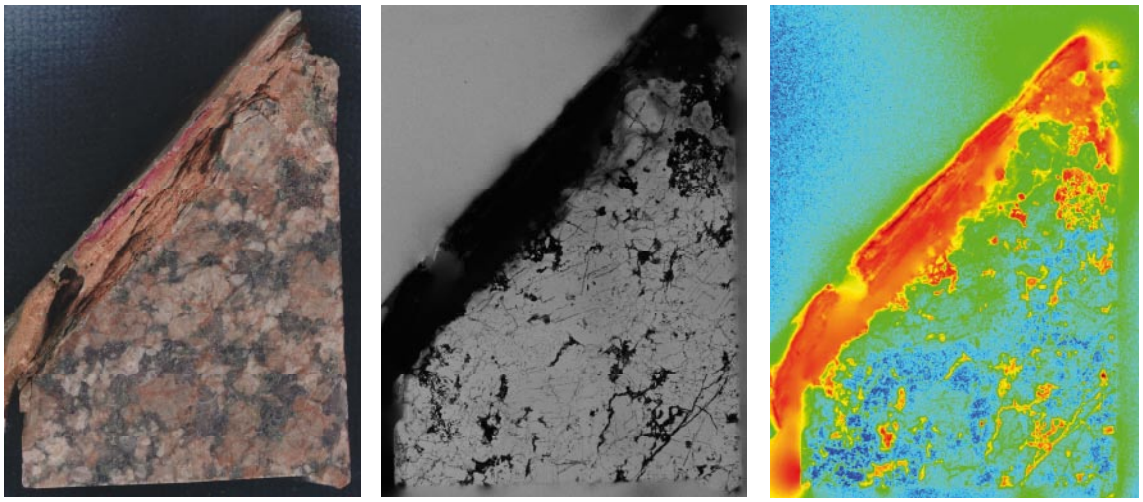

a *b* *c*

Figure 5-14. *a) the analysed rock surface of sample O6A, b) its corresponding film autoradiograph and c) its corresponding digital autoradiograph.*

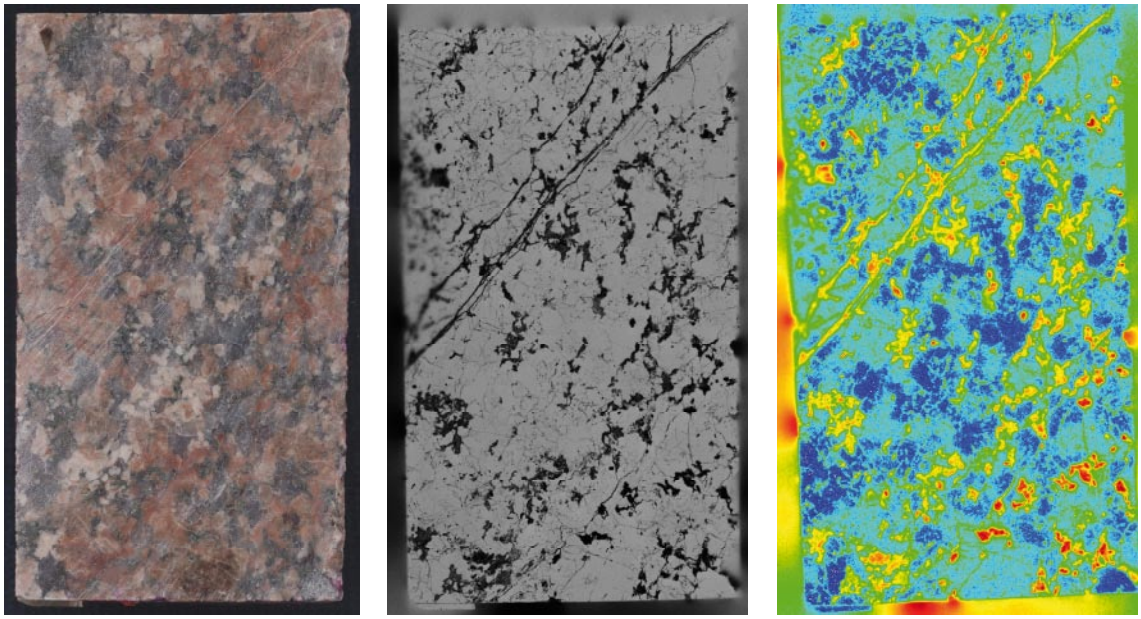

a *b* *c*

Figure 5-15. *a) the analysed rock surface of sample O6B, b) its corresponding film autoradiograph and c) its corresponding digital autoradiograph.*

The PMMA porosity of the sample O6 was 0.5%. Figures 5-16 and 5-17 show the porosity histograms for O6A and O6B (7d exposure time) achieved with the PMMA method. There are some porous mineral phases (> 3% porosity, see Figure 5-18) found sparsely distributed in the rock below the highly porous fracture coating material. The connections between the porous phases are visualised in 2D by PMMA when long exposure time is used. The grain boundaries are filled with MMA and tiny features indicate pore apertures of micrometer scale. A filled fracture transects the rock sample and a porosity of 3% is found in the filling material of this fracture.

The highly porous fracture surface coating was problematic when impregnating this sample. Highly porous samples are usually irradiated under ^{14}C-MMA to avoid out diffusion of tracer from rock during the irradiation polymerisation step. This was not done with sample O6A because the low initial porosity of the matrix did not suggest doing so. The reason for surrounding the sample with MMA during irradiation is also to avoid the decomposition of the highly porous matrices due to shrinking of MMA when it polymerises. Sample O6A had this highly porous (> 10% porosity) clayish fracture coating, which has decomposed in the polymerisation step (see Figure 5-14a).

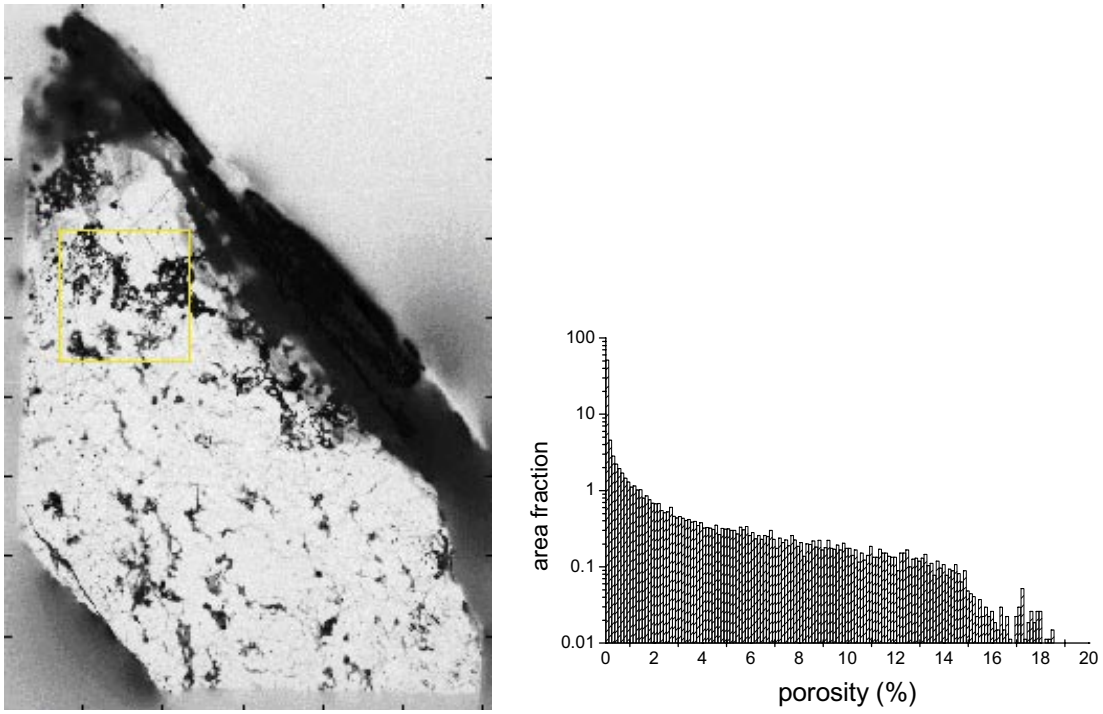

Figure 5-16. *Porosity histogram of sample O6A. A total PMMA porosity of about 2% was determined.*

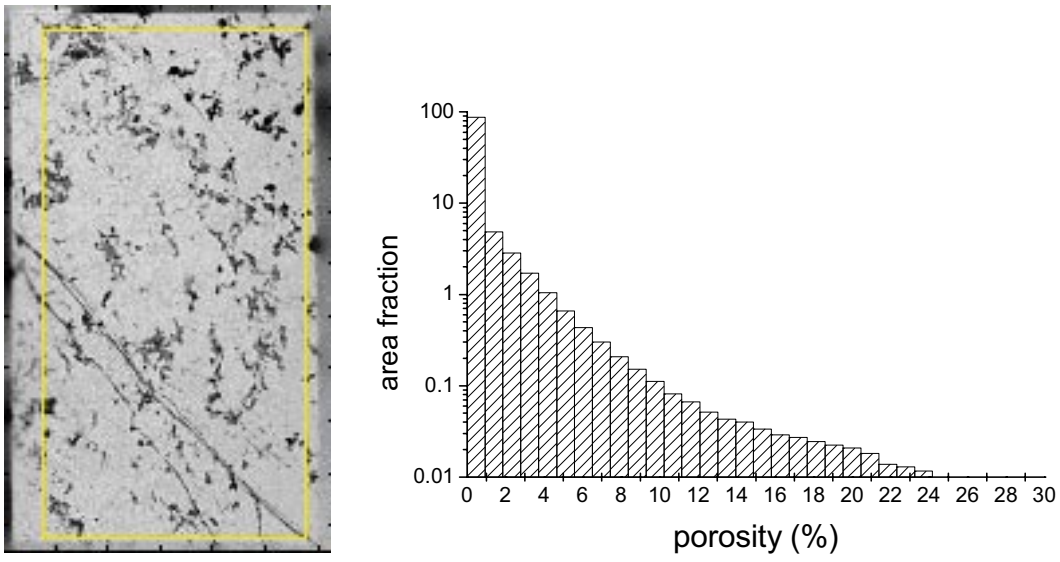

Figure 5-17. *Porosity histogram of sample O6B. A total PMMA porosity of about 0.5% was determined.*

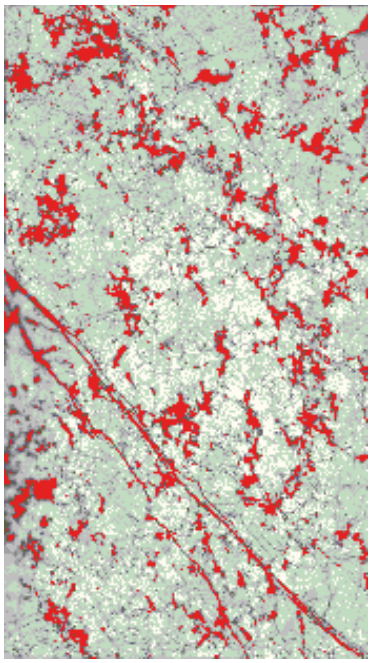

Figure 5-18. *Autoradiograph of sample O6B with porosities of over 3% shown in red.*

5.7 Sample O7 (KSH02)

The photograph taken of sample O7, before any operation, and the partition diagram are presented in Appendix 7. After impregnation the sample was sawn into two pieces. Photo images of the analysed rock surfaces after impregnation and sawing for samples O7A and O7B are presented below in Figures 5-19a and 5-20a, the corresponding film and digital autoradiographs are shown in Figures 5-19b, 5-19c and 5-20b, 5-20c, respectively. The exposure time on the film autoradiograph was 21 days and on the digital autoradiograph 3 days.

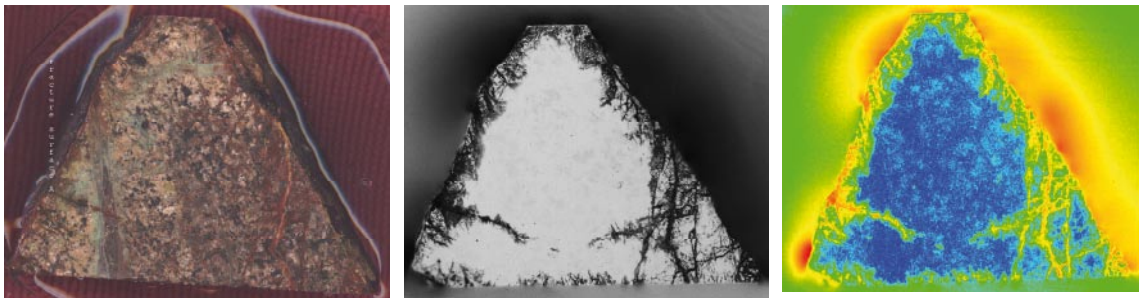

a *b* *c*

Figure 5-19. *a) the analysed rock surface of sample 07A, b) its corresponding film autoradiograph and c) its corresponding digital autoradiograph. The fracture surface A is on the left.*

a *b* *c*

Figure 5-20. *a) the analysed rock surface of sample O7B, b) its corresponding film autoradiograph and c) its corresponding digital autoradiograph. The farcture surface B is on the right.*

The PMMA porosity for sample O7, in areas where the ^{14}C-MMA had intruded, varied between 1% and 3%. The porosity of the filling material in fractures was about 3–5%. Figures 5-22, 5-23 and 5-24 show the porosity histograms achieved with the PMMA method for the areas on O7B indicated in Figure 5-21. The rock sample has not been fully impregnated, inner parts of the rock piece were non porous with PMMA technique indicating very low permeable matrix. A very tight altered matrix was found, filled fissures transecting the rock pieces.

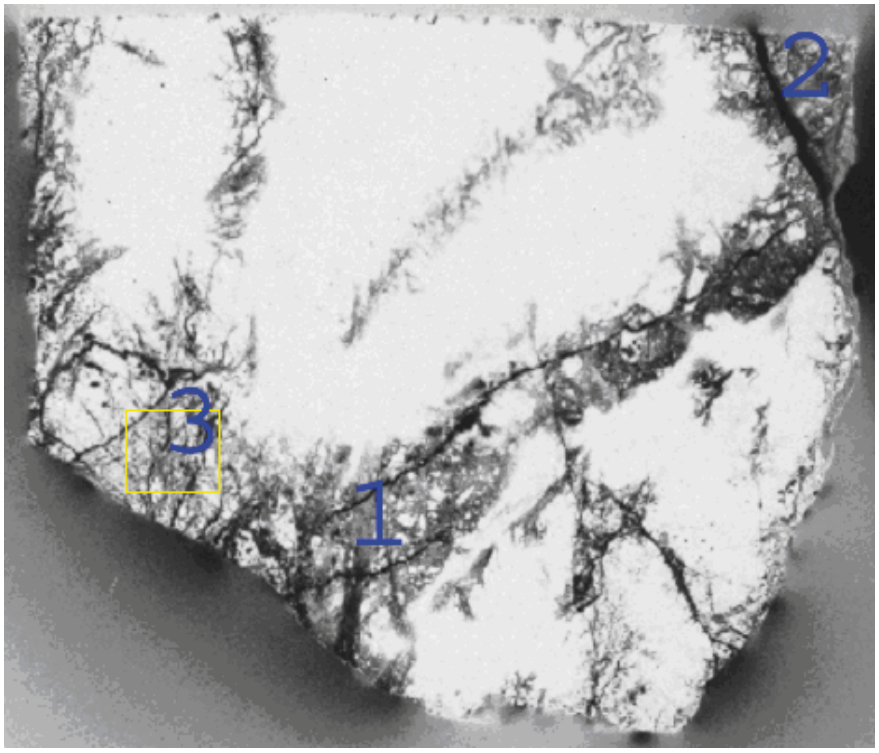

Figure 5-21. *Porous regions of sample 07B used in the porosity histograms.*

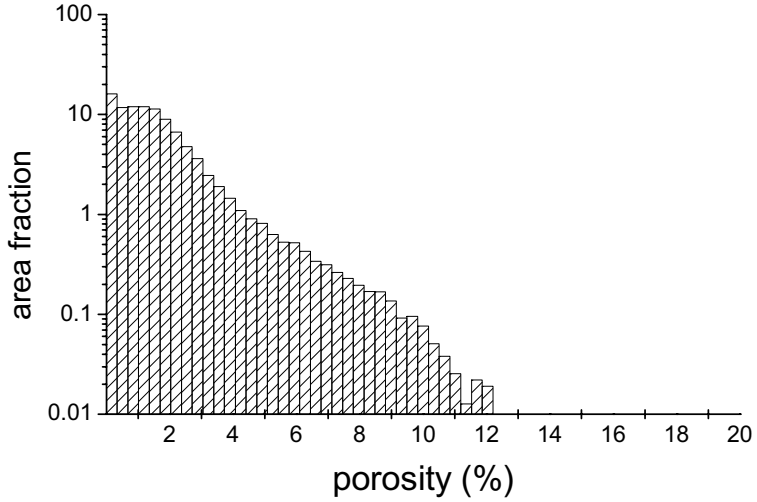

Figure 5-22. *Porosity histogram of sample O7 area 1. A total PMMA porosity of 1.7% was determined.*

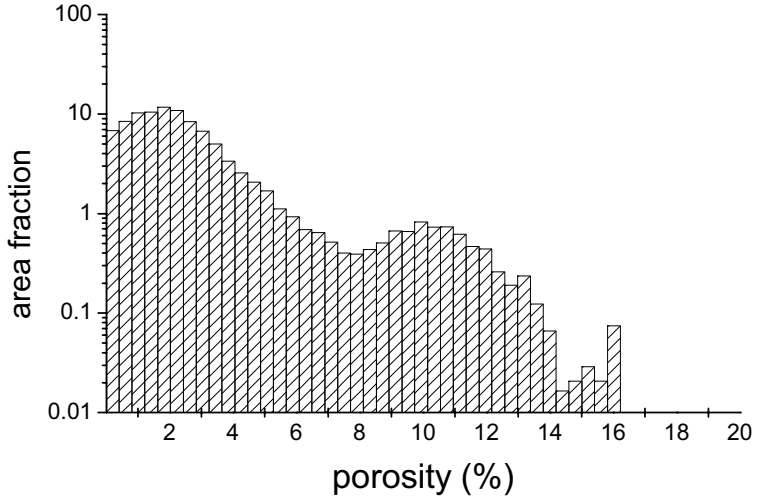

Figure 5-23. *Porosity histogram of sample O7 area 2. A total PMMA porosity of 2.8% was determined.*

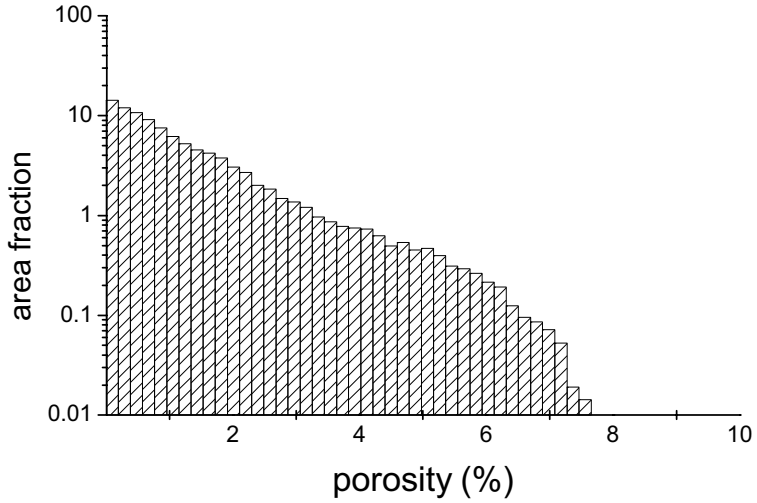

Figure 5-24. *Porosity histogram of sample O7 area 3. A total PMMA porosity of 1.2% was determined.*

5.8 Sample O8 (KSH02)

The photograph taken of sample O8, before any operation and the partition diagram are presented in Appendix 8. A photo image of the analysed rock surface after impregnation and sawing is presented below in Figure 5-25a and the corresponding film and digital autoradiographs are shown in Figures 5-25b and 5-25c, respectively. The exposure time on the film autoradiograph was 6 days and on the digital autoradiograph 23 hours.

The PMMA porosity for the sample O8 was 3%. Figures 5-26 and 5-27 show the porosity histograms for O8 achieved with the PMMA method from the areas indicated in the same figures. The sample has been fully impregnated with MMA and the porosity pattern is found to be strongly heterogeneous. Highly porous veins surrounding mineral clusters showing low PMMA porosity, can be seen on the autoradiograph. The low porous mineral areas seen on the autoradiograph contain tightly packed medium grained altered mineral clusters that cannot be clearly separated from the photo image of the corresponding rock surface. Strongly altered and weathered matrix shows an uneven porosity distribution. In Figure 5-28 porosities of over 10% are emphasized with red colour. Some of the features are congruent with the mineral cluster grain boundaries which are a bit open.

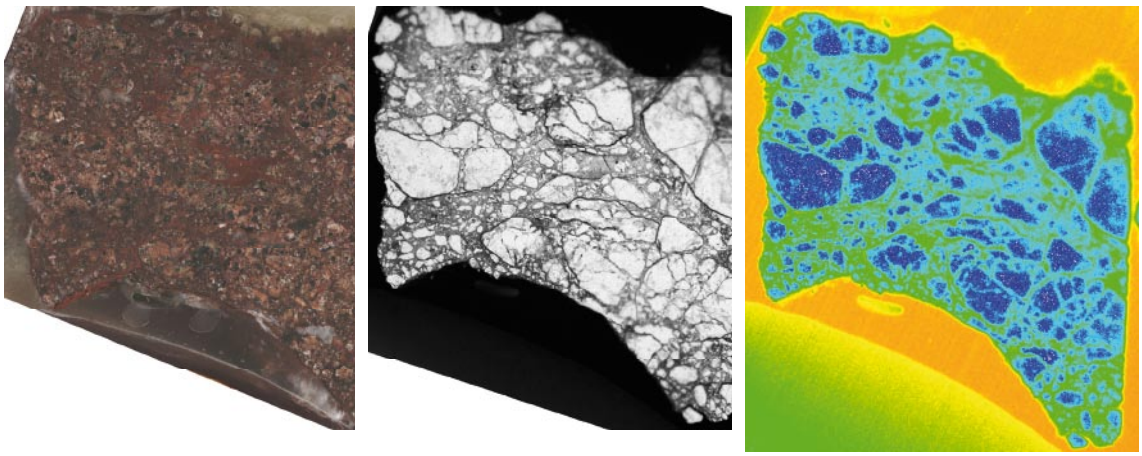

a *b* *c*

Figure 5-25. *a) the analysed rock surface of sample O8, b) its corresponding film autoradiograph and c) its corresponding digital autoradiograph.*

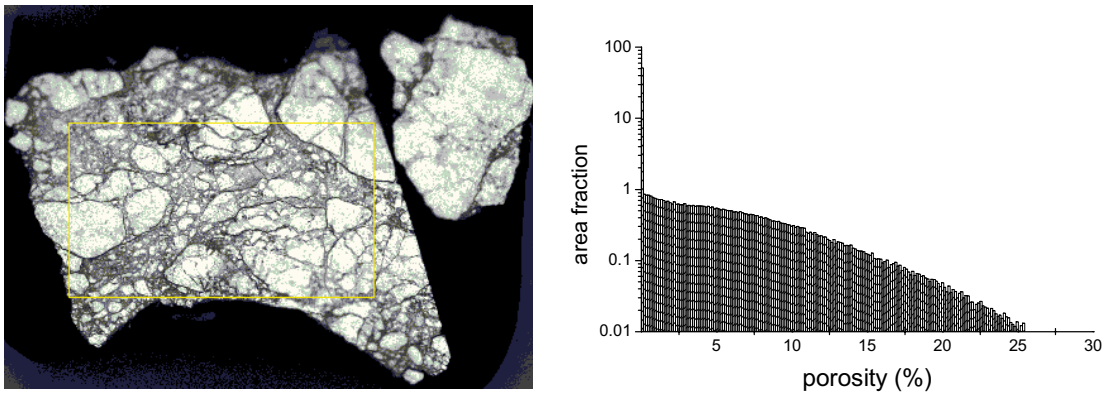

Figure 5-26. *Porosity histogram for the indicated part of sample O8. A total PMMA porosity of 3% was determined.*

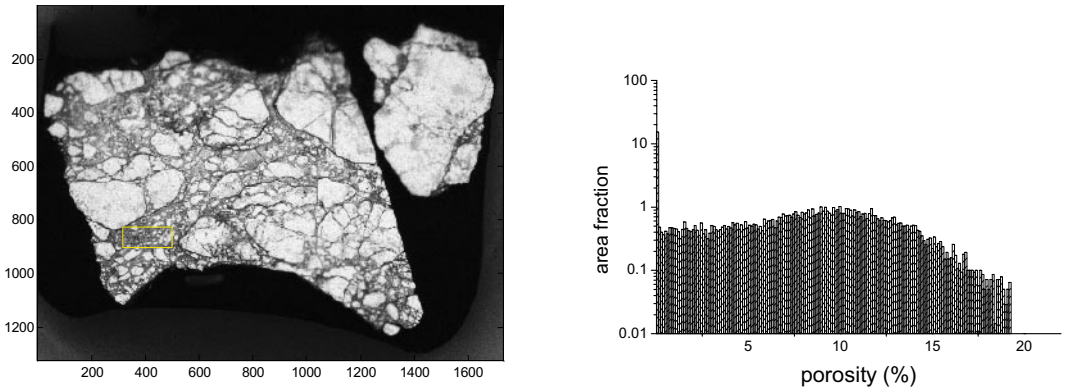

Figure 5-27. *Porosity histogram for the indicated part of sample O8. A total PMMA porosity of 8% was determined*

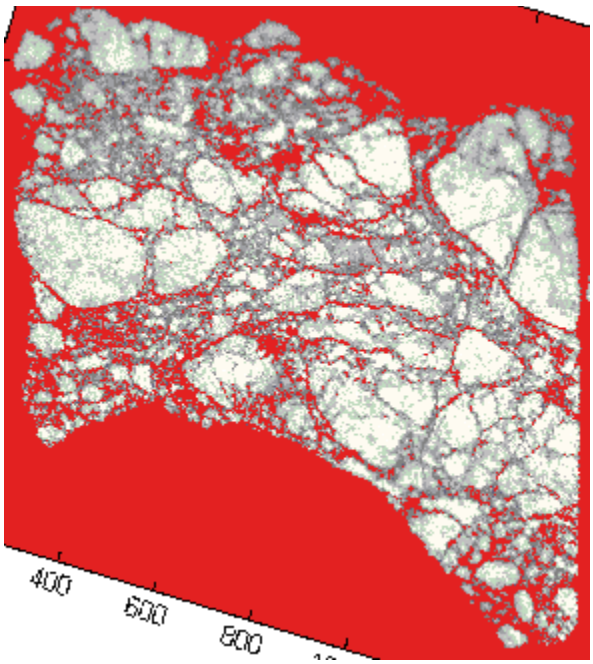

Figure 5-28. *Autoradiograph of sample O8 with porosities of over 10% shown in red.*

5.9 Sample O9 (KLX02)

The photograph taken of sample O9, before any operation, and the partition diagram are presented in Appendix 9. A photo image of the analysed rock surface after impregnation and sawing is presented below in Figure 5-29a and the corresponding film and digital autoradiographs are shown in Figures 5-29b and 5-29c, respectively. The exposure time on the film autoradiograph was 6 days and on the digital autoradiograph 21 hours.

The PMMA porosity of the sample O9 was about 5–10% depending strongly on the measured mineral phase. The porosity of the rock matrix is low varying from 0.5 to 1%. The porosity pattern was found heterogeneous. Figures 5-30 and 5-31 show the porosity histograms for O9 achieved with the PMMA method from the areas indicated in the same figures. The rock sample has been fully impregnated with MMA. The pore structure is congruent with the altered chlorite phases (the greenish color on the rock) and is visualised clearly on the autoradiograph. The altered clay phases form a connective network of highly porous veins (over 20% porosity). In Figure 5-32 porosities of over 20% are emphasized in red colour.

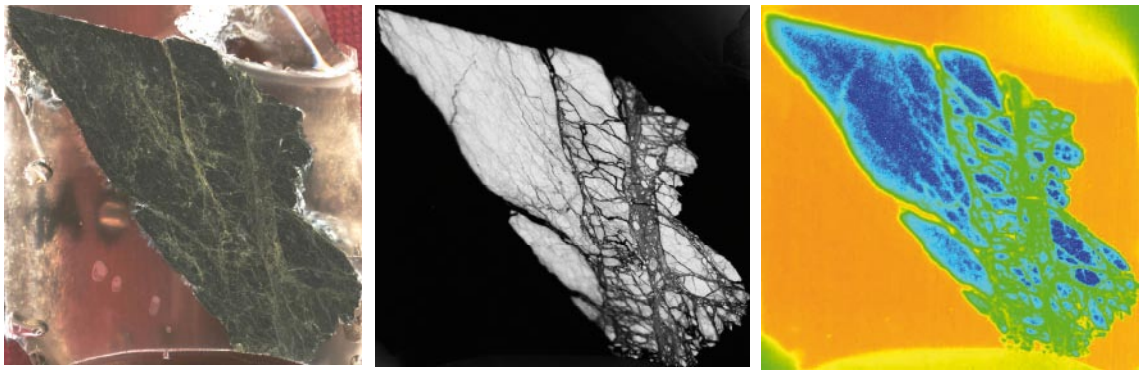

a *b* *c*

Figure 5-29. *a) the analysed rock surface of sample O9, b) its corresponding film autoradiograph and c) its corresponding digital autoradiograph.*

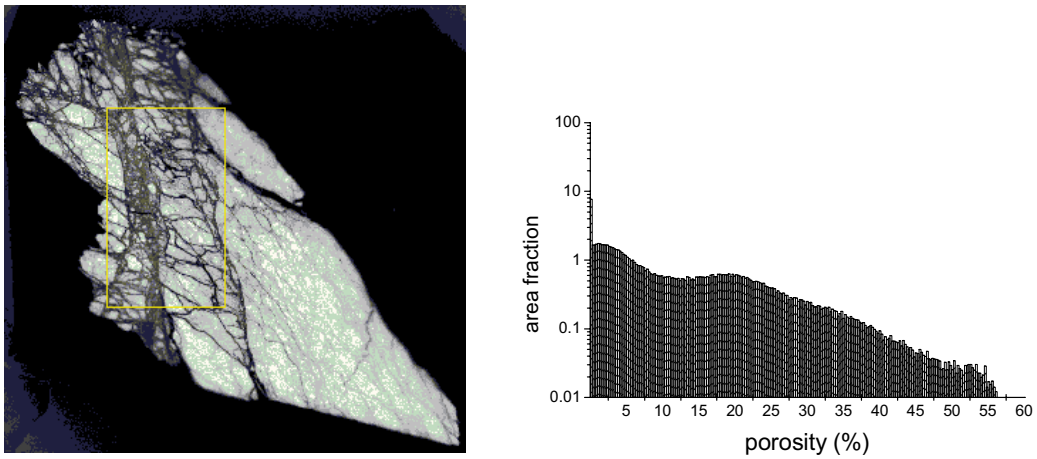

Figure 5-30. *Porosity histogram of sample O9. Total PMMA porosity of 12% was determined.*

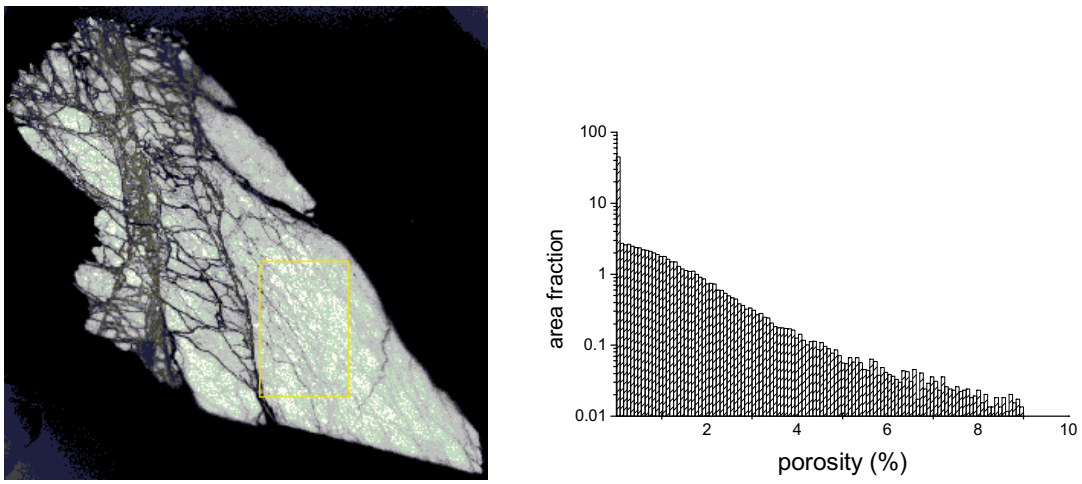

Figure 5-31. *Porosity histogram for the indicated area of sample O9. A total PMMA porosity of 0.8% was determined.*

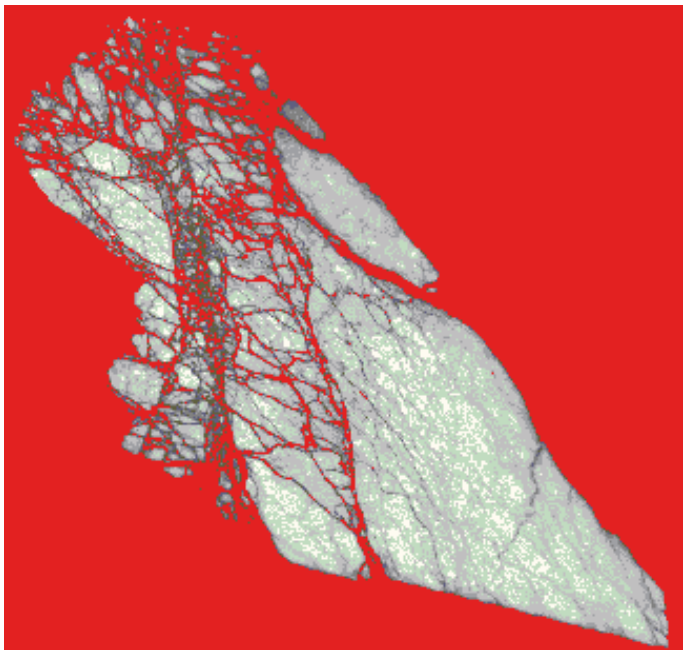

Figure 5-32. *Autoradiograph of sample O9 with porosities of over 10% shown in red.*

5.10 Sample O10 (KLX03)

The photograph taken of sample O10, before any operation, and the partition diagram are presented in Appendix 10. The photo images of the analysed rock surfaces (small test piece and the PMMA.sample) after impregnation and sawing are presented below in Figures 5-33a and 5-34a, the corresponding film and digital autoradiographs for 5-33a are shown in Figures 5-33b and 5-33c, and for 5-34a in Figures 5-34b and 5-34c, respectively. The exposure time on the film autoradiograph was 8 days and on the digital autoradiograph 23 hours.

The PMMA porosity for the sample O10 was about 4%. Due to heterogeneous porosity pattern the porosity value differed for mineral phases strongly according to the determined region on the autoradiograph. The ground matrix on the other hand has a porosity of about 0.5%. Both the O10 and O10 test sample were irradiated under ^{14}C-MMA. Figure 5-35a shows the area used for determining the total porosity histogram for the O10 sample illustrated in Figure 5-35b. Within this area there are highly porous phases, including cracks and fractures.

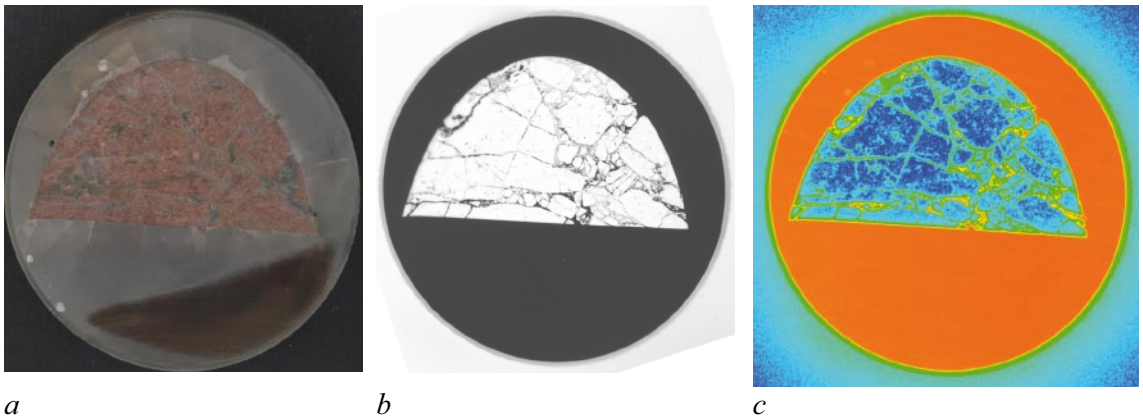

a *b* *c*

Figure 5-33. *a) the analysed rock surface of the test piece O10, b) its corresponding film autoradiograph and c) its corresponding digital autoradiograph.*

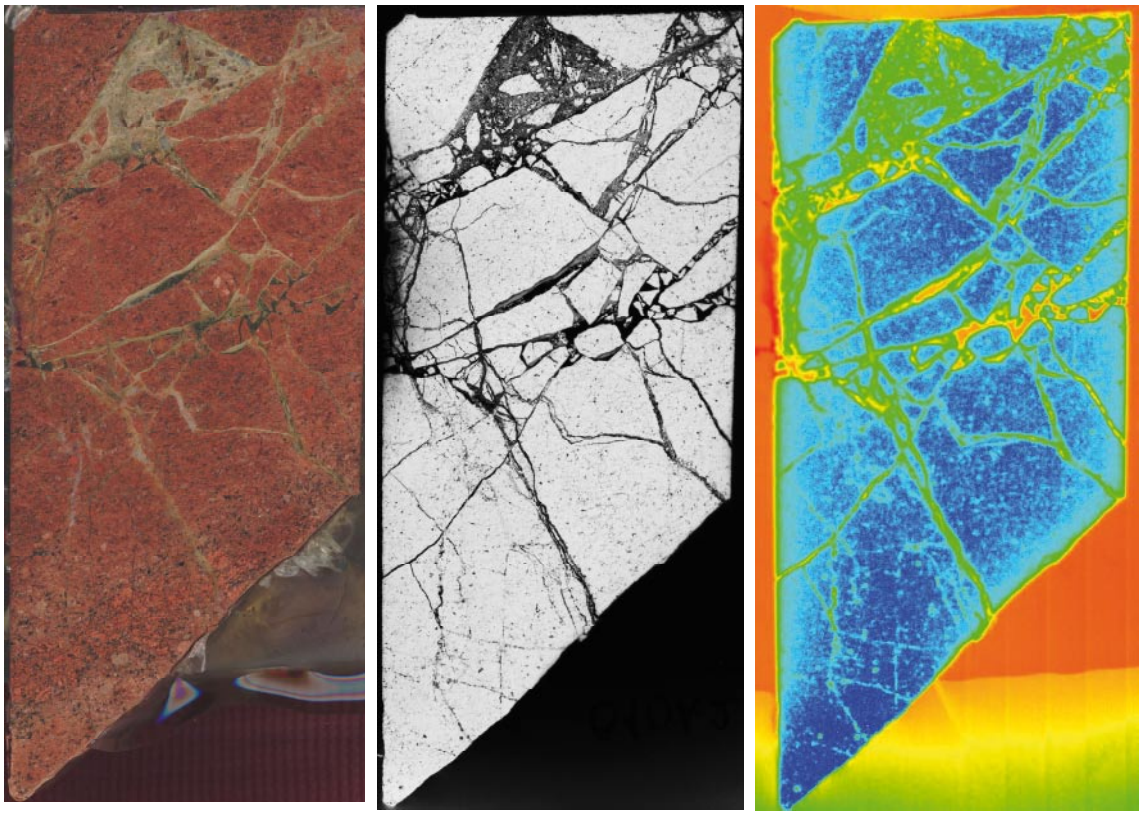

a *b* *c*

Figure 5-34. *a) the analysed rock surface of sample O10, b) its corresponding film autoradiograph and c) its corresponding digital autoradiograph.*

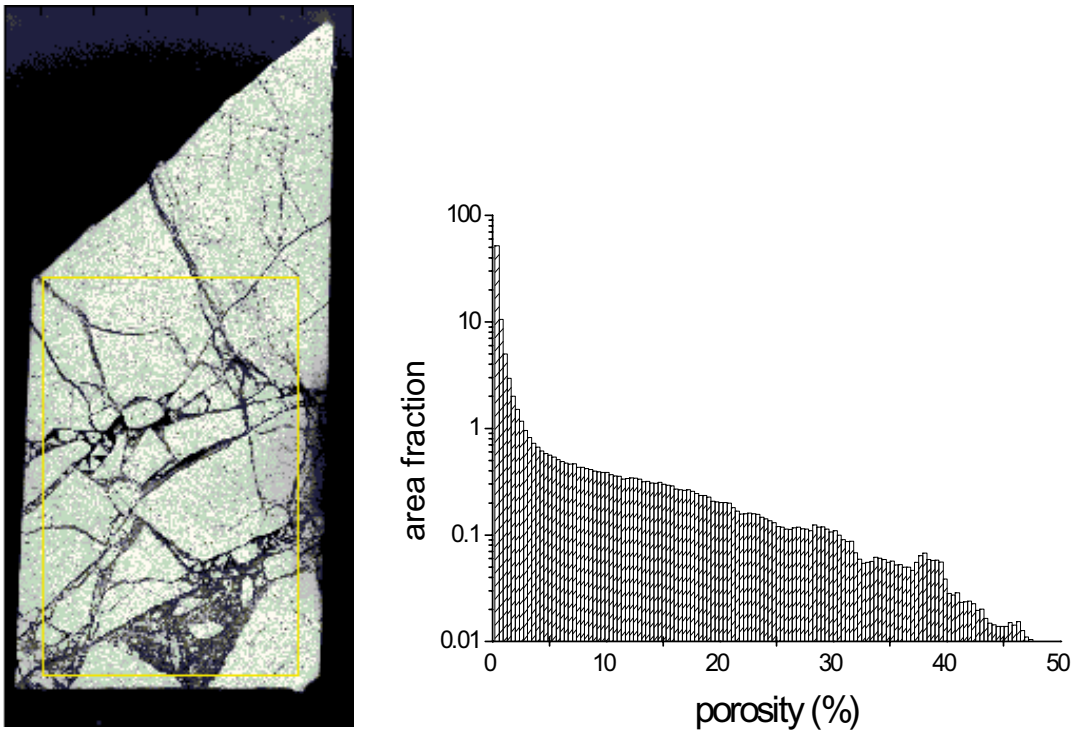

Figure 5-35. *Porosity histogram for the indicated area of sample O10. A total PMMA porosity of 4% was determined.*

In Figures 5-36a and 5-37a a magnification of the rock surface image can be seen. Their corresponding film autoradiographs are presented in Figures 5-36b and 5-37b, respectively. In these images the different porosity associated with some mineral are emphasized and now open veins are seen within these mineral phases.

Figure 5-36. *a) a magnification of a porous region of sample O10, where three different phases are clearly shown.*

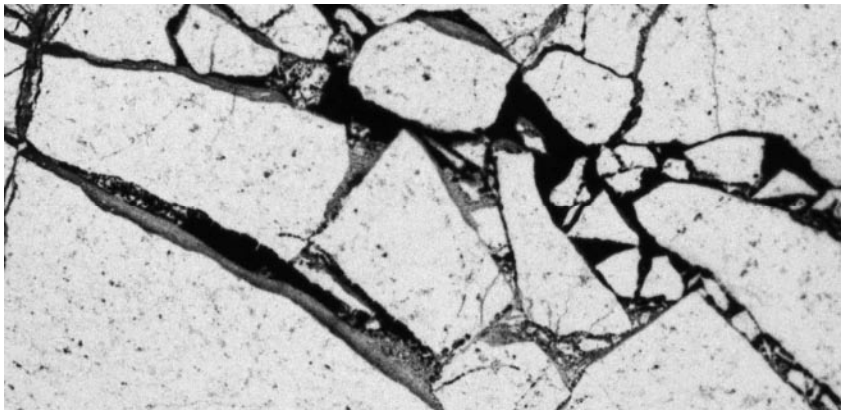

Figure 5-36. *b) corresponding autoradiograph of sample O10 showing different porosities in the three phases.*

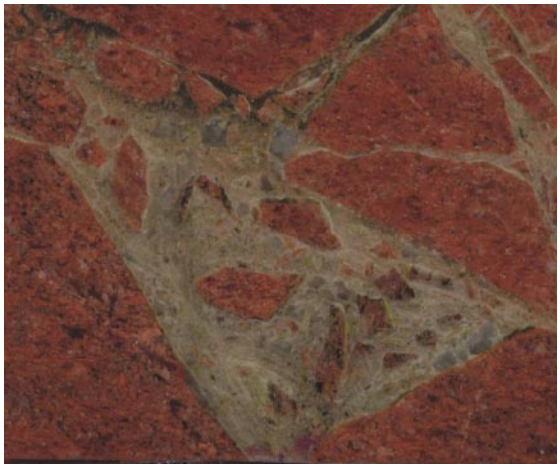

Figure 5-37. *a) a magnification of porous phases of sample O10.*

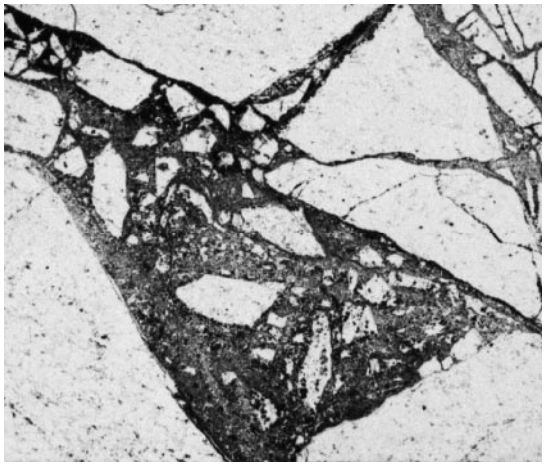

Figure 5-37. *b) corresponding autoradiograph of sample O10.*

5.11 Sample O11 (KLX04)

The photograph taken of sample O11, before any operation, and the partition diagram are presented in Appendix 11. A photo image of the analysed rock surface after impregnation and sawing is presented below in Figure 5-38a and the corresponding film and digital autoradiographs are shown in Figures 5-38b and 5-38c, respectively. The exposure time on the film autoradiograph was 14 days and on the digital autoradiograph 4 days.

The PMMA porosity for the sample O11 was 0.15–0.25%. Figure 5-39 shows a porosity histogram for O11 achieved with the PMMA method from the area indicated in the same figure. The rock sample has been fully impregnated and is clearly showing a heterogeneous porosity pattern. Most of the minerals were non porous with the PMMA technique. Grain boundary porosity dominates and the porous areas are congruent with mafic minerals existing around feldspar grains. Numerous micro fractures transect the core parallel to the fracture surface. Parallel micro fractures are connected with micro fractures perpendicular to the surface to a depth of 1–2 cm from the surface. The porosity profile, presented in Figure 5-40; shows an increased porosity zone to a depth of about 1.5 cm from fracture surface.

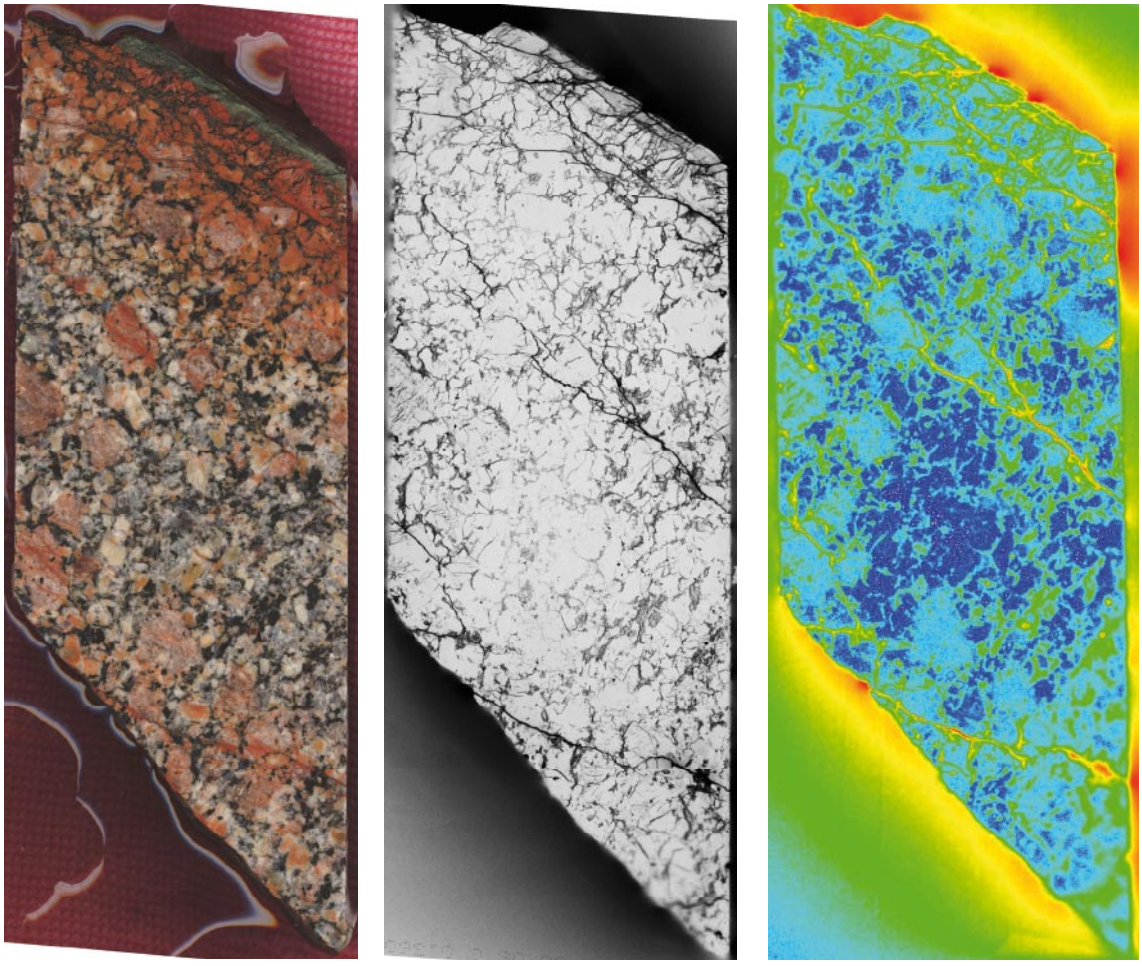

a *b* *c*

Figure 5-38. *a) the analysed rock surface of sample O11, b) its corresponding film autoradiograph and c) its corresponding digital autoradiograph.*

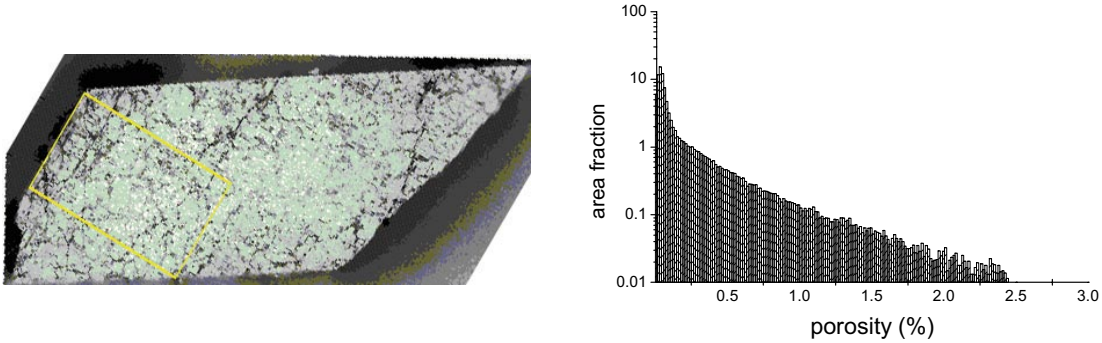

Figure 5-39. *Porosity histogram for the indicated area of sample O11. Total PMMA porosity of 0.25% was determined.*

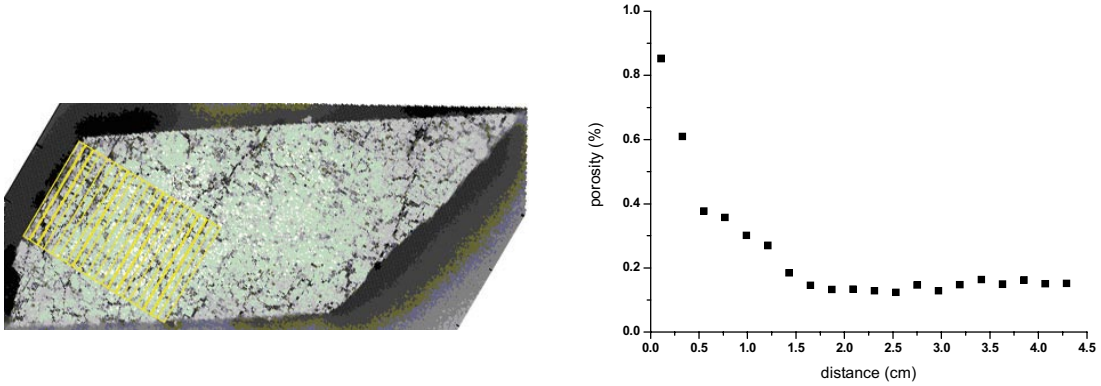

Figure 5-40. *Porosity profile for sample O11.*

5.12 Sample O12 (KLX04)

The photograph taken of sample O12, before any operation, and the partition diagram are presented in Appendix 12. After impregnation the sample was sawn in two pieces. The photo images of the analysed rock surfaces after impregnation and sawing for samples O12A and O12B are presented below in Figures 5-41a and 5-42a and the corresponding film and digital autoradiographs for sample O12A are shown in Figures 5-41b and 5-41c, and for sample O12B in Figures 5-42b and 5-42c, respectively. The exposure time on the film autoradiograph was 7 days and on the digital autoradiograph 23 hours.

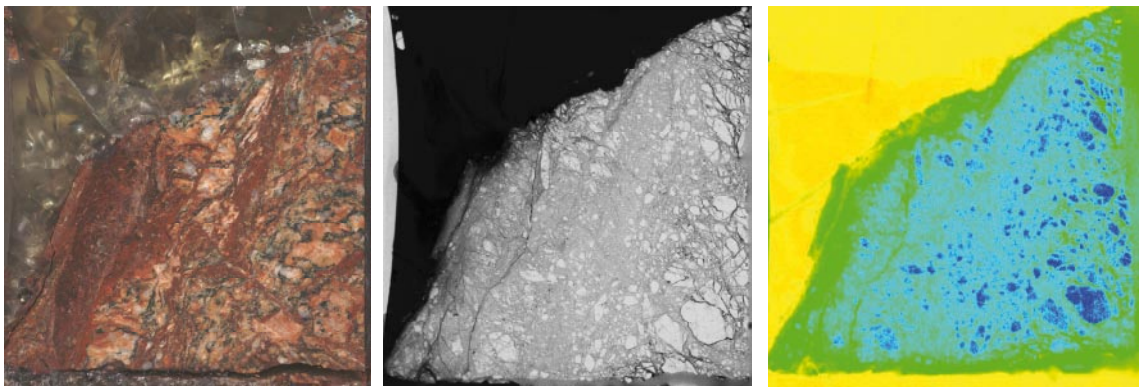

a *b* *c*

Figure 5-41. *a) the analysed rock surface of sample O12A, b) its corresponding film autoradiograph and c) its corresponding digital autoradiograph.*

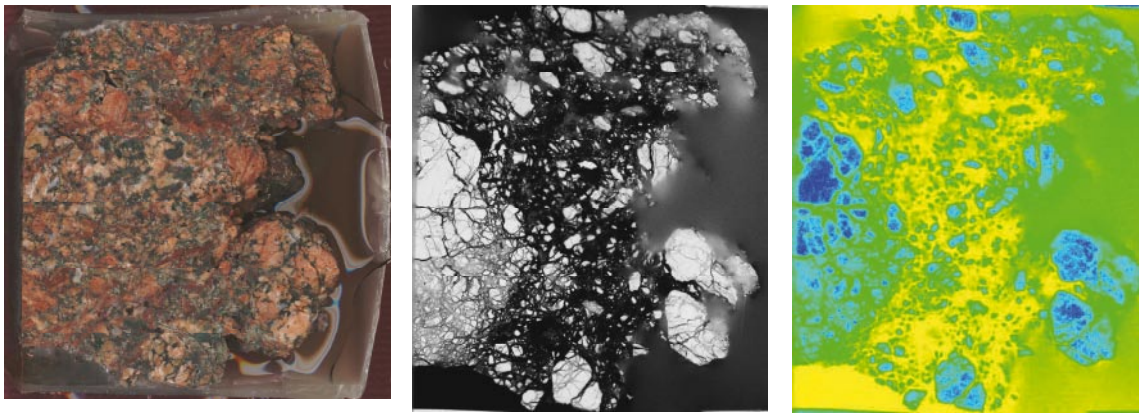

a *b* *c*

Figure 5-42. *a) the analysed rock surface of sample O12B, b) its corresponding film autoradiograph and c) its corresponding digital autoradiograph.*

The PMMA porosity for sample O12 was about 5–6% in phases that were not broken during irradiation polymerisation. The O12 sample was irradiated under ^{14}C-MMA. The sample has been fully impregnated but the most porous parts are broken due to shrinking during the irradiation. The parts that have broken are highly porous.

O12A shows an even porosity pattern. Most of the minerals were found to be porous, the grain boundary pores as well as micro fractures transecting the large mineral grains found on the opposite site from the facture surface. Figure 5-43 shows a porosity histogram for one phase of O12A. Figure 5-44 shows a porosity profile starting from the fracture surface. An increased porosity zone was found roughly to a depth of 1 cm.

In the upper part of sample O12B the grain boundary pores as well as micro fractures transecting the large mineral grains can be seen. Highly porous mineral grains were found from the lower parts of the sample (Figures 5-43 and 5-44). In these parts the PMMA porosity measurement (over 40% porosity) can only be seen as indicative.

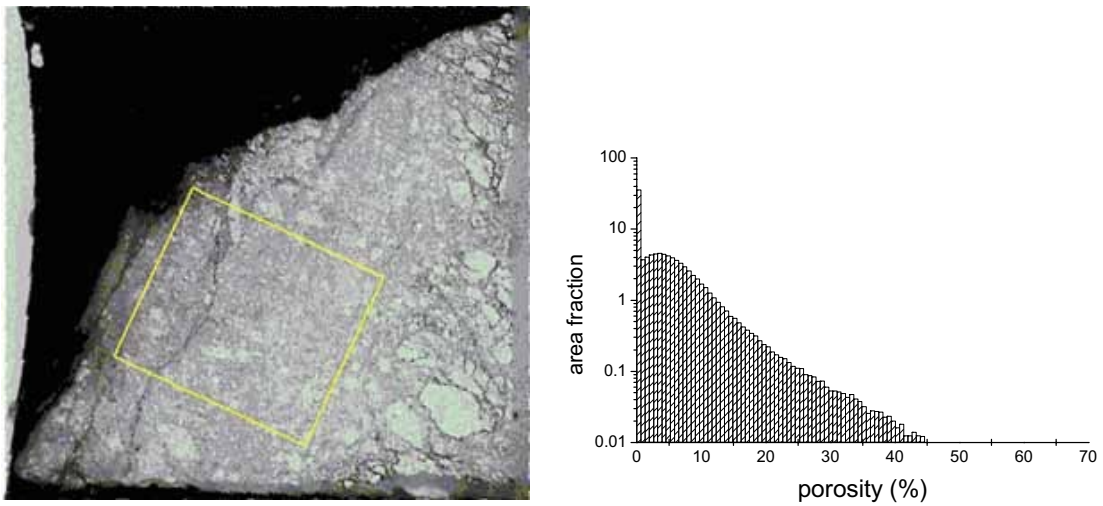

Figure 5-43. *Porosity histogram for the indicated area of sample O12A. Total PMMA porosity of 5.6% was determined.*

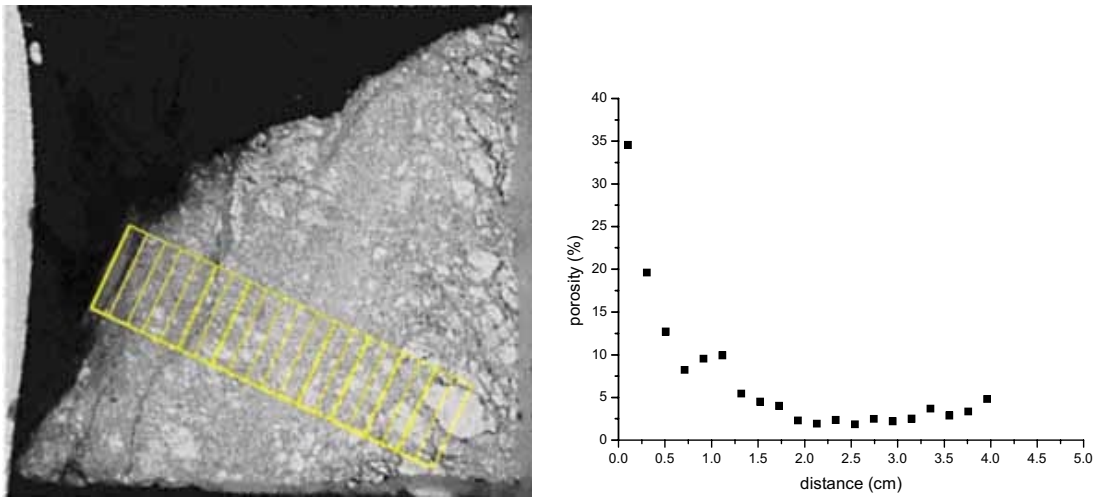

Figure 5-44. *Porosity profile for sample O12A.*

5.13 Sample O13 (KLX05)

The photograph taken of sample O13, before any operation, and the partition diagram is presented in Appendix 13. A photo image of the analysed rock surface after impregnation and sawing is presented below in Figure 5-45a and the corresponding film and digital autoradiographs are shown in Figures 5-45b and 5-45c, respectively. The exposure time on the film autoradiograph was 20 days and on the digital autoradiograph 2 days.

Figure 5-45 shows that the sample O13 is non porous with the PMMA-method. ^{14}C-MMA has not intruded at all into the rock matrix indicating low permeability. With water gravimetry the porosity for sample O13 H_2O was 0.1%.

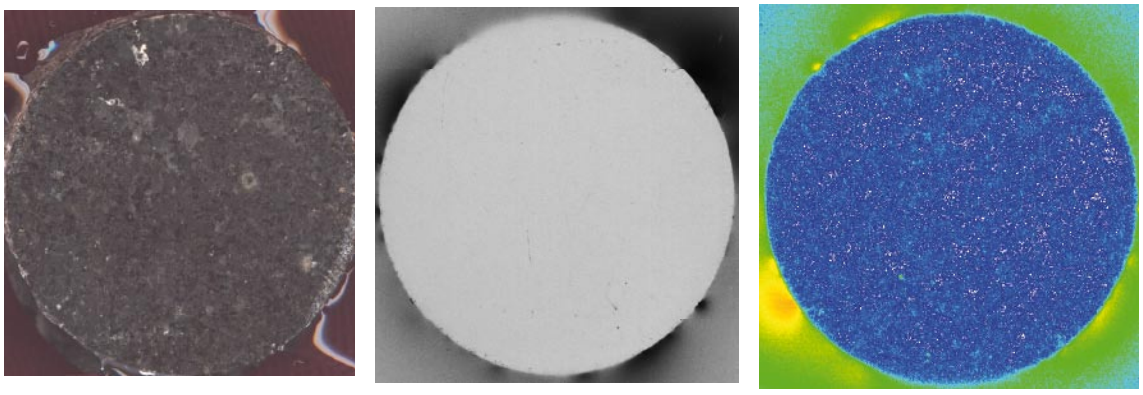

a *b* *c*

Figure 5-45. *a) the analysed rock surface of sample O13, b) its corresponding film autoradiograph and c) its corresponding digital autoradiograph.*

5.14 Sample O14 (KLX05)

The photograph taken of sample O14, before any operation, and the partition diagram are presented in Appendix 14. A photo image of the analysed rock surface after impregnation and sawing is presented below in Figure 5-46a and the corresponding film and digital autoradiographs are shown in Figures 5-46b and 5-46c, respectively. The exposure time on the film autoradiograph was 20 days and on the digital autoradiograph 2 days.

The PMMA porosity for the sample O14 was 0.1%. Figure 5-47 shows the porosity histogram for O14 achieved with the PMMA method. The rock sample has been impregnated, slightly porous veins have been visualised. The porosity pattern shows slight foliation. With water gravimetry the porosity for sample O14 H_2O was 0.2%.

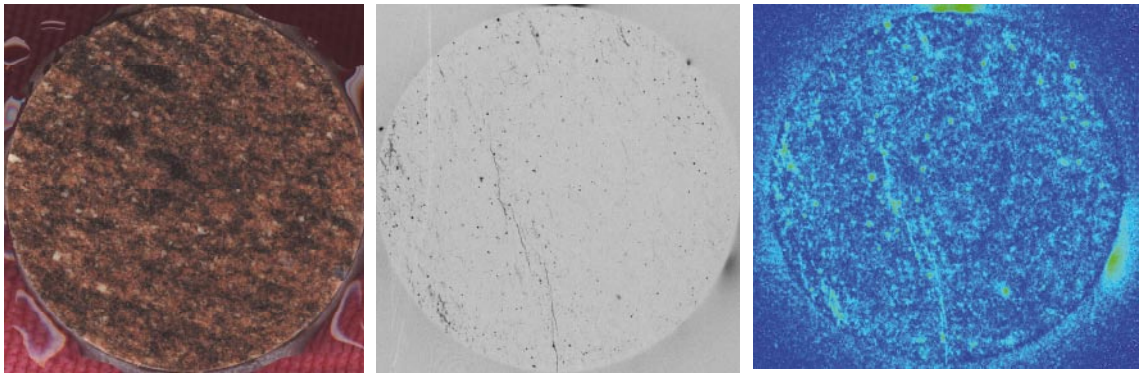

a *b* *c*

Figure 5-46. *a) the analysed rock surface of sample O14, b) its corresponding film autoradiograph and c) its corresponding digital autoradiograph.*

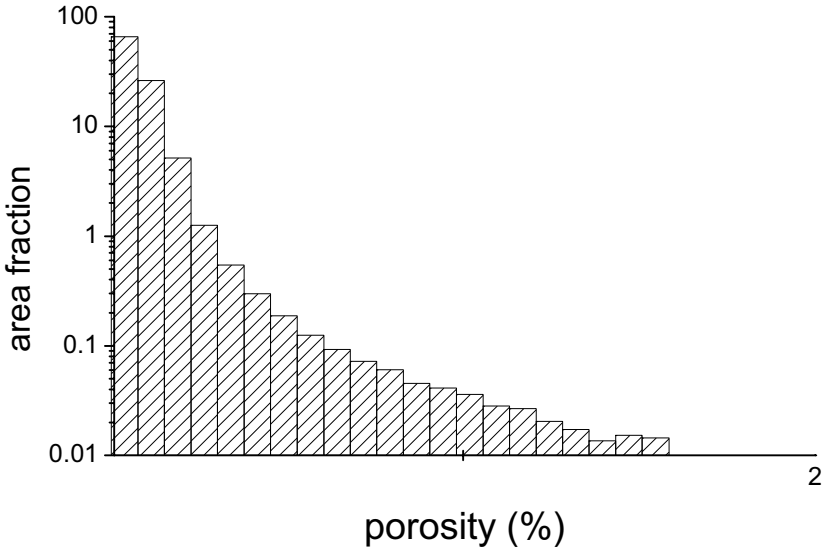

Figure 5-47. *Porosity histogram of sample O14. A total PMMA porosity of 0.1% was determined.*

5.15 Sample O15 (KLX06)

The photograph taken of sample O15, before any operation, and the partition diagram are presented in Appendix 15. A photo image of the analysed rock surface after impregnation and sawing is presented below in Figure 5-48a and the corresponding film and digital autoradiographs are shown in Figures 5-48b and 5-48c, respectively. The exposure time on the film autoradiograph was 15 days and on the digital autoradiograph 4 days.

The PMMA porosity for the sample O15 was 0.3%. Figure 5-49 shows the total porosity histogram for O15 achieved with the PMMA method from the area indicated in the same figure. The rock sample has been fully impregnated. The micro fractures cutting the sample were clearly visualised with the PMMA technique. When the branched micro fractures were excluded from the PMMA measurement the porosity varied from 0.1% to 0.2%. With water gravimetry the porosity for sample O15 was 0.6%.

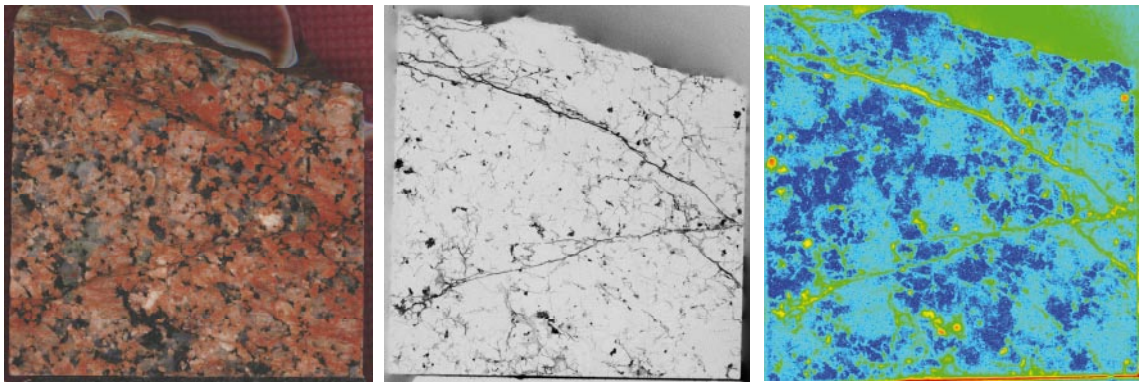

a *b* *c*

Figure 5-48. *a) the analysed rock surface of sample O15, b) its corresponding film autoradiograph and c) its corresponding digital autoradiograph.*

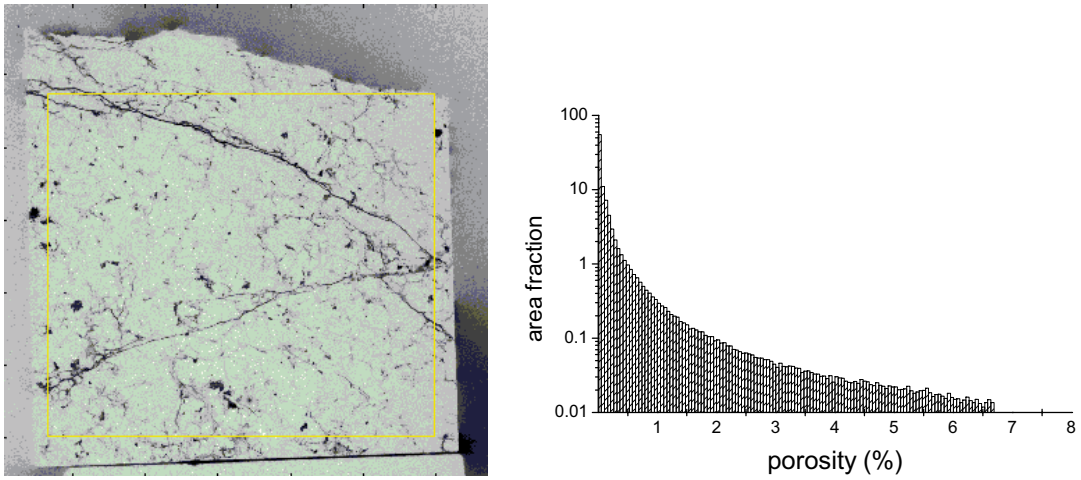

Figure 5-49. *Porosity histogram of sample O15. A total PMMA porosity of 0.3% was determined.*

5.16 Sample O16 (KSH02)

The photograph taken of sample O16, before any operation, and the partition diagram are presented in Appendix 16. A photo image of the analysed rock surface after impregnation and sawing is presented below in Figure 5-50a and the corresponding film and digital autoradiographs are shown in Figures 5-50b and 5-50c, respectively. The exposure time on the film autoradiograph was 25 days and on the digital autoradiograph 4 days.

Most of the sample O16 was non porous with PMMA method indicating a very tight structure. The impregnated phase showed 1.5% porosity. This porous zone extended to a depth of 1–2 cm from the fracture surface. The porous zone consists of highly porous mafic mineral grains. Figure 5-51 shows the porosity histogram for O16 achieved with the PMMA method from the area indicated in the same figure. A branched fracture was found to cut the rock core. A few micro fractures appeared parallel to the fracture surface at depths of 1–2 cm from the fracture surface.

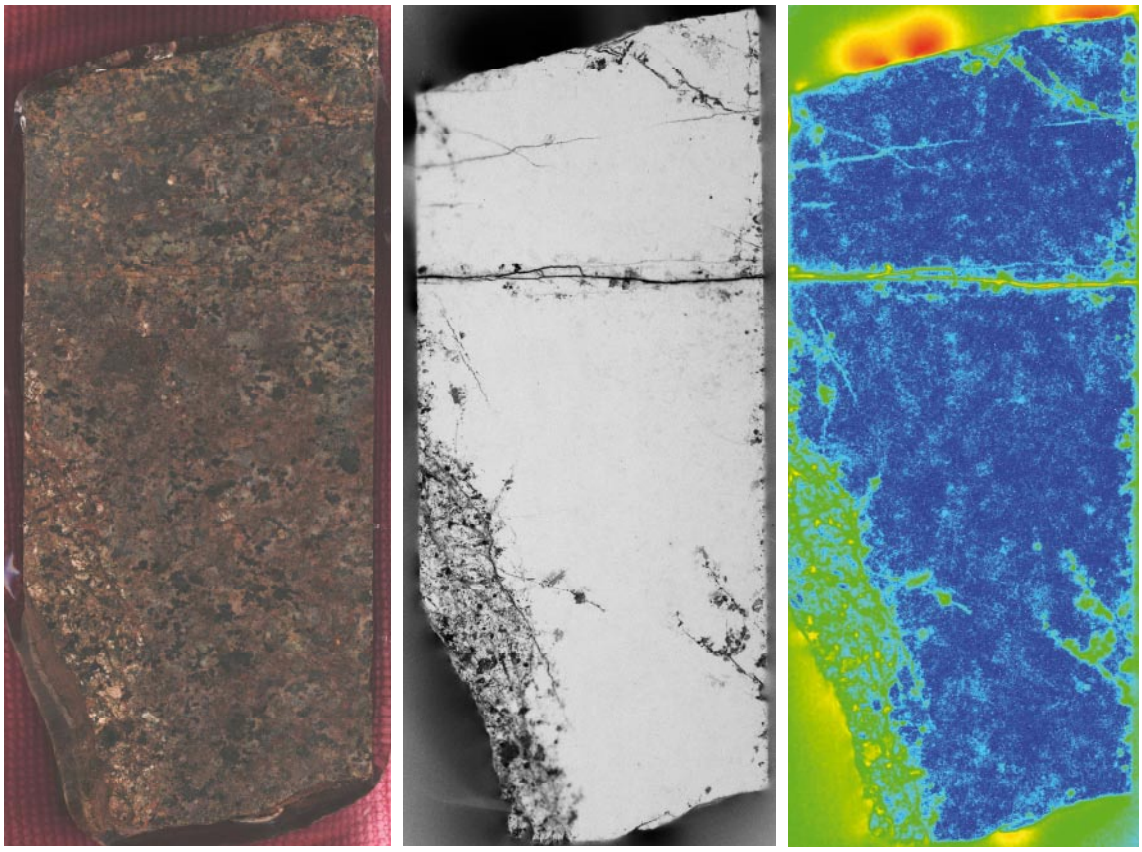

a *b* *c*

Figure 5-50. *a) the analysed rock surface of sample O16, b) its corresponding film autoradiograph and c) its corresponding digital autoradiograph.*

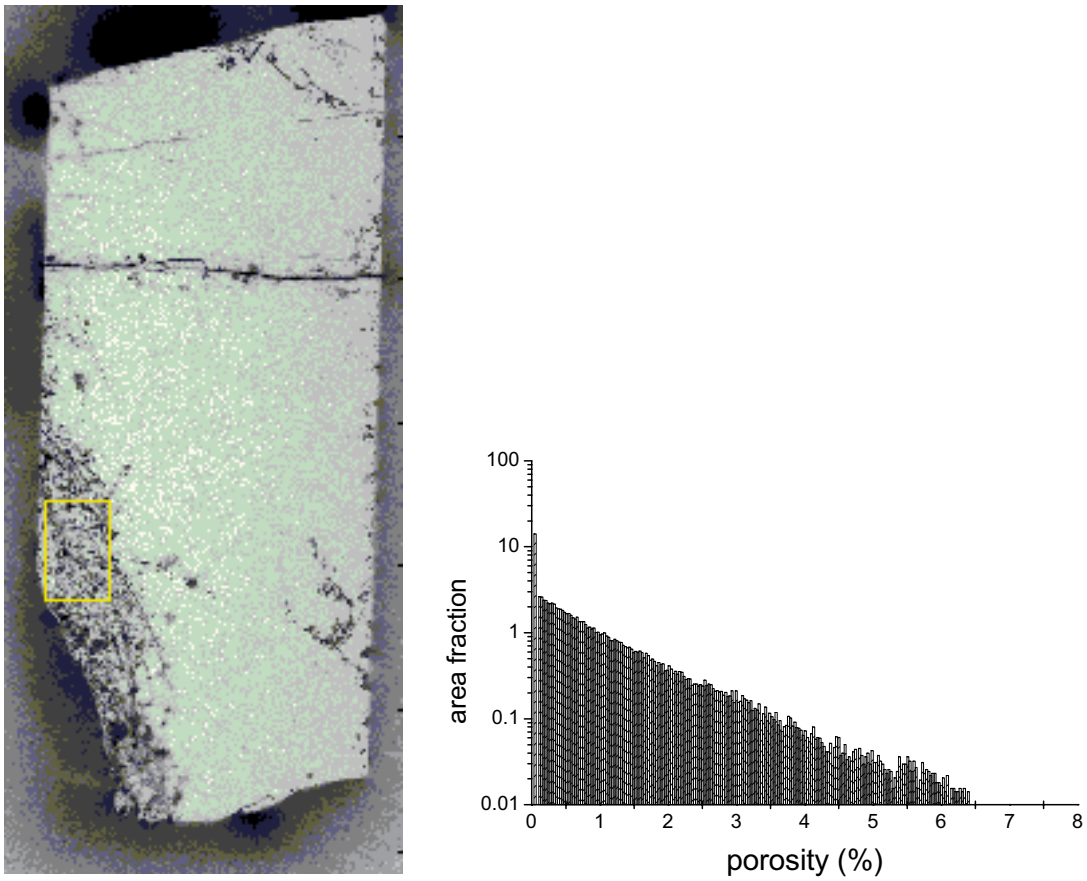

Figure 5-51. *Porosity histogram for the indicated area of sample O16. A total PMMA porosity of 1.5% was determined.*

6 Summary and discussions

Sixteen crystalline rock samples were analysed by the ^{14}C-PMMA method. The method involves impregnation of centimetre-scale rock cores with ^{14}C-labelled methylmethacrylate (^{14}C-MMA) in a vacuum, irradiation polymerisation, sample partitioning, autoradiography, optical densitometry and porosity calculation routines using digital image processing techniques.

The samples included different crystalline rock types from the Simepvarp and the Laxemar site investigation areas. In addition a few samples were taken adjacent to possibly water bearing fracture zones. The PMMA porosities for the low porous rock matrices, i.e. porosities lower than 1%, varied between 0.03% and 0.8% depending on the sample. These samples represent quartz monzodiorites, monzodiorites, diorites, granites and gabbros; fine to medium grained unaltered or altered rocks. For example samples O8, O9 and O12 contained altered rock matrix and PMMA porosity was high; 3–20%, indicating very permeable rock.

The main focus of the work was to analyse the porosities and visualise the heterogeneous pore structure of crystalline rocks by using ^{14}C-PMMA autoradiographs. However in many cases the porosity pattern was not congruent with the mineral texture. The intragranular porosity dominated in samples having high porosities. These samples had also very heterogeneous porosity patterns in cm scales. The experiences from this study have shown that the technique can be applied effectively to study the spatial distribution of porosity in the low porous media. The porosity profiles adjacent to water bearing fracture zones can also be studied.

As thought in the beginning of the PMMA method development, the MMA molecule is considered to behave as a neutral particle in rock, without strong surface interaction, and it can be roughly compared with water. The presence of residual water and the surface state of the rock pore space are influenced by the pre-treatment (drying and decassing) that the samples undergo before impregnation. Intrusion of MMA, which is a hydrophobic fluid, is hindered if even thin water layers remain absorbed on the rock pore surfaces after drying. The initial expectation was that the above mentioned differences could cause some discrepancy in the porosity values obtained by the PMMA method and water gravimetry. Correlations between water and PMMA porosities are plotted in Figure 6-1. The PMMA porosity values were in most of the cases lower than the porosity values from water gravimetry /5/. Relative to water gravimetry the PMMA method underestimates the porosity values by 10 to 40%.

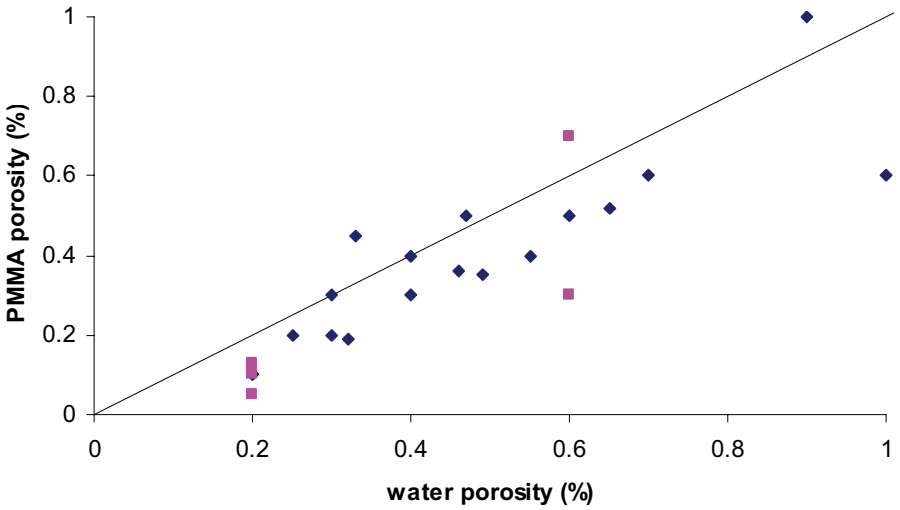

Figure 6-1. *Porosity values from water gravimetry compared with PMMA results for all studied rock samples by Siitari-Kauppi /5/ (blue squares) and in this work (red squares).*

There are three probable reasons for the lower porosity values measured by the PMMA method. First, the MMA molecule, in contrast to water, may not intrude into the smallest pores of the rock matrix, thus decreasing the porosity values. The finding that the PMMA porosity values are in disagreement with the water porosity values in unaltered rocks, suggests incomplete intrusion of MMA into the narrow pore spaces. Secondly, the sensitivity of the PMMA method is directly dependent on the signal detection, initially the blackening of the autoradiograph, which is dependent on the ^{14}C activity in the rock, and then the image digitising and on the linearity requirement of the digitising equipment. Thus, if the threshold energy for the autoradiography is not exceeded, some concentration of MMA in the rock may go undetected, resulting in the recording lower porosity values by the PMMA method than by water gravimetry. Thirdly, if the nonlinear region of the calibration curve is used in the PMMA method, the uncertainty for high porosity values increases and possibly lowering the total PMMA porosities.

7 References

/*1*/ **Hellmuth K-H, Siitari-Kauppi M, Lindberg A, 1993.** Study of Porosity and Migration Pathways in Crystalline Rock by Impregnation With ^{14}C-Polymethylmethacrylate, Journal of Contaminant Hydrology 13, 403–418.

/2/ **Hellmuth K-H, Lukkarinen S, Siitari-Kauppi M, 1994.** Rock Matrix Studies with Carbon-14-Polymethylmethacrylate (PMMA): Method Development and Applications. Isotopenpraxis. Isotopes in Environmental and Health Studies 30, 47–60.

/3/ **Hellmuth K-H, Siitari-Kauppi M, Klobes P, Meyer K, Goebbels J, 1999.** Imaging and Aanalyzing Rock Porosity by Autoradiography and Hg-Porosimetry/X-ray Computertomography-Applications, Phys. Chem. Earth (A), Vol. 24, No. 7, 569–573.

/4/ **Siitari-Kauppi M, Flitsiyan E S, Klobes P, Meyer K, Hellmuth K-H, 1998.** Progress in Physical Rock Matrix Characterization: Structure of the Pore Space. In: I.G. McKinley, C. McCombie (edits.), Scientific Basis for Nuclear Waste Management XXI, Mat. Res. Soc. Symp. Proc. 506, 671–678.

/5/ **Siitari-Kauppi M, 2002.** Development of ^{14}C-Polymethylmethacrylate Method to Characterise Low Porosity Media-Application to Rocks in Geological Barriers of Nuclear Waste Storage. Academic Thesis, UHRAD-17-2002.

/6/ **Siitari-Kauppi M, Autio J, 2001.** Study of Rock Damage by Drill and Blast Excavation at the Research Tunnel at Olkiluoto, In Water-Rock Interaction 10, Cidu (ed) Balkema, Lisse, 1387–1390.

/7/ **Autio J, Kirkkomäki T, Siitari-Kauppi M, Laajalahti M, Aaltonen T, Maaranen J, 1999.** Use of the ^{14}C-PMMA and He-gas Methods to Characterise Excavation Disturbance in Crystalline Rock, Posiva 99-22 & SKB Report IPR-99-18.

/8/ **Daniels F, Alberty R A, 1967.** Physical Chemistry, Third Edition, John Wiley & Sons, Inc. New York, 384 (767).

/9/ **Leonard E C, 1978.** Vinyl and diene monomers, Part 1, A Series of Monographs on the Chemistry, Physics, and Technology of High Polymeric Substances, Vol. XXIV, 157.

/10/ **Frieg B, Alexaner W R, Dollinger H, Buhler C, Haag P, Möri A, Ota K, 1998.** In Situ Resin Impregnation or Investigating Radionuclide Retardation in Fractured Repository Host Rocks, Journal of Contaminant Hydrology 35, 115–130.

Appendix 1

Worksheet for sample O1 (KSHO1)

The photo images of sample O1 before any operation and the partition map for PMMA analyses and autoradiography. Shaded surfaces are autoradiographed.

Figure A1-1. *The whole sample before analysis.*

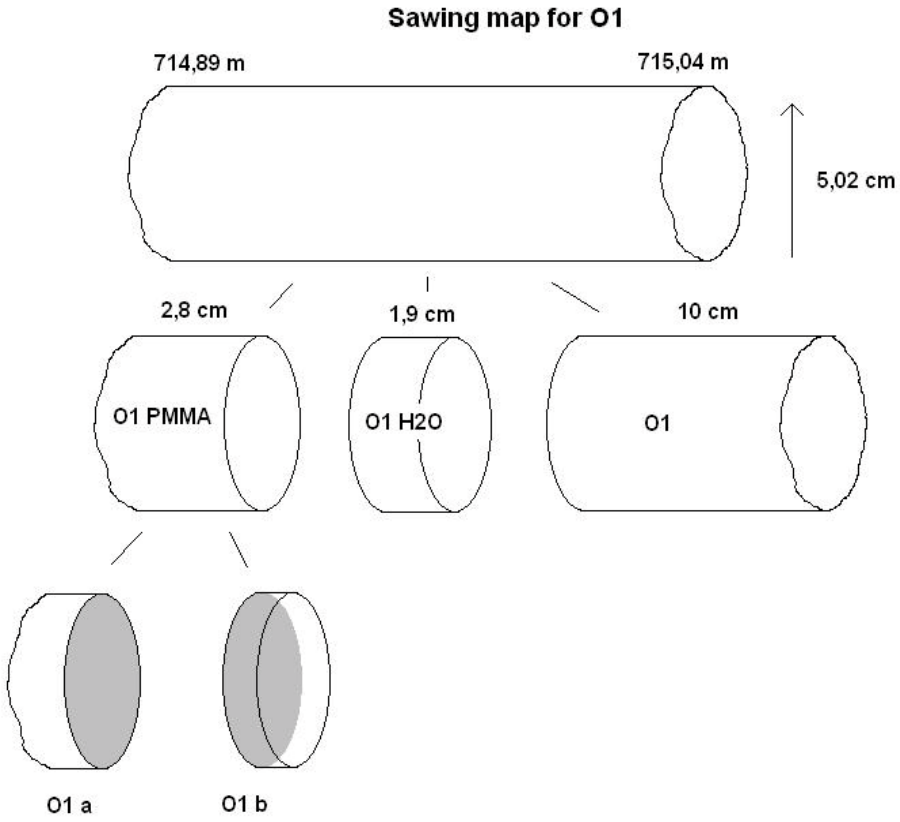

Figure A1-2. *Partition diagram for sample O1.*

Appendix 2

Worksheet for sample O2 (KSHO2)

The photo images of sample O2 before any operation and the partition map for PMMA analyses and autoradiography. Shaded surfaces are autoradiographed.

Figure A2-1. *The whole sample before analysis. Lengths were later adjusted and correct lengths are given in Figure A2-2.*

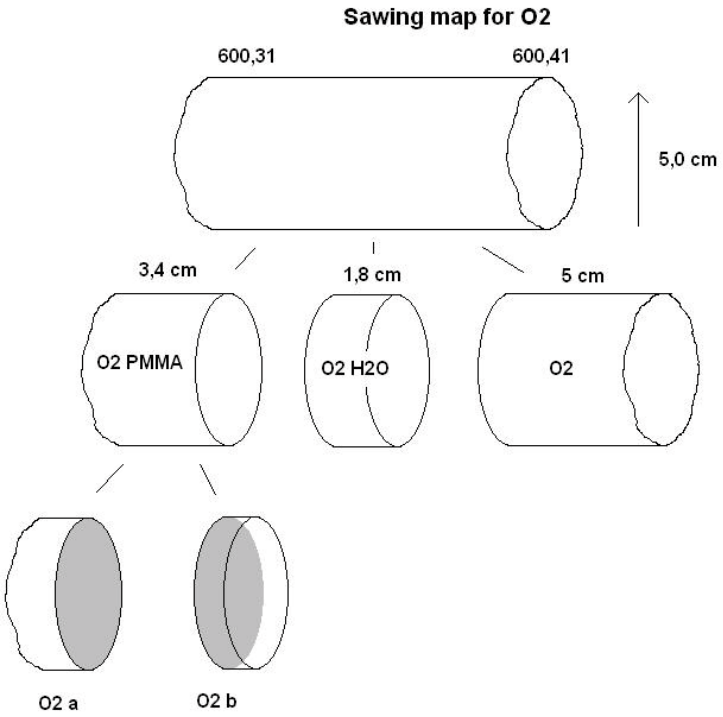

Figure A2-2. *Partition diagram for sample O2.*

Appendix 3

Worksheet for sample O3 (KLXO2)

The photo images of sample O3 before any operation and the partition map for PMMA analyses and autoradiography. Shaded surfaces are autoradiographed.

Figure A3-1. *The whole sample before analysis.*

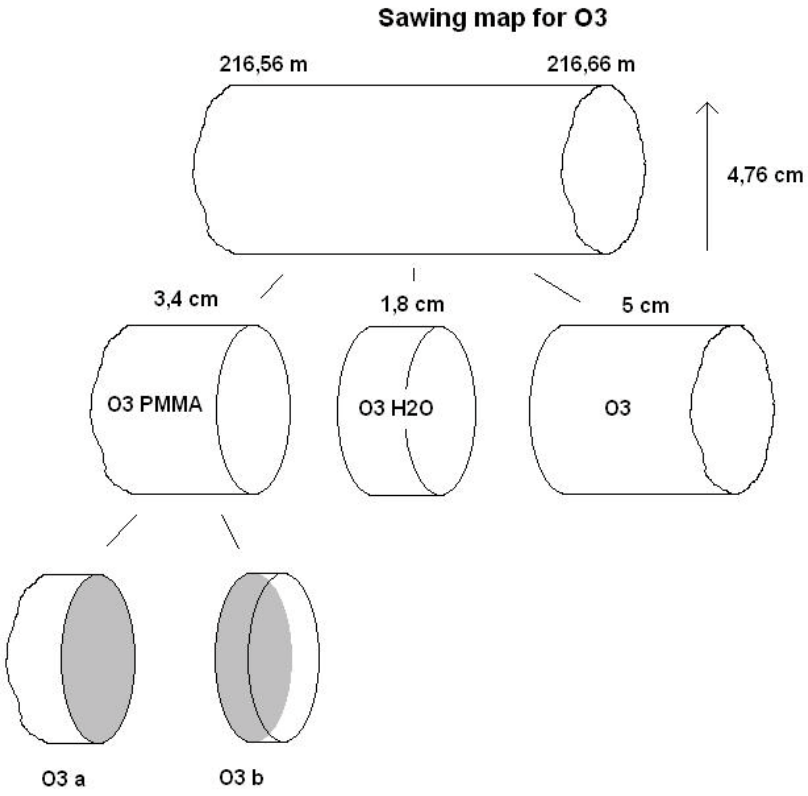

Figure A3-2. *Partition diagram for sample O3.*

Appendix 4

Worksheet for sample O4 (KLXO2)

The photo images of sample O4 before any operation and the partition map for PMMA analyses and autoradiography. Shaded surfaces are autoradiographed.

Figure A4-1. *The whole sample before analysis.*

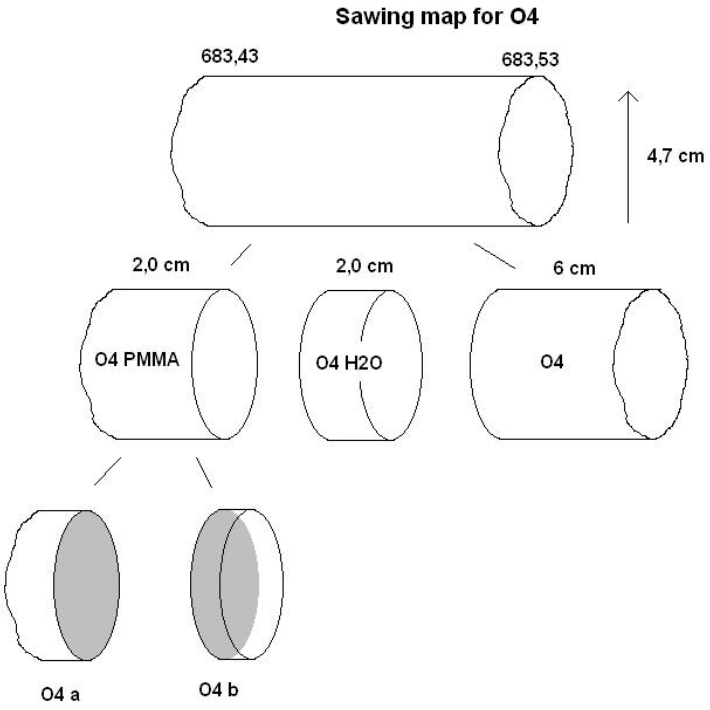

Figure A4-2. *Partition diagram for sample O4.*

Appendix 5

Worksheet for sample O5 (KLXO6)

The photo images of sample O5 before any operation and the partition map for PMMA analyses and autoradiography. Shaded surfaces are autoradiographed.

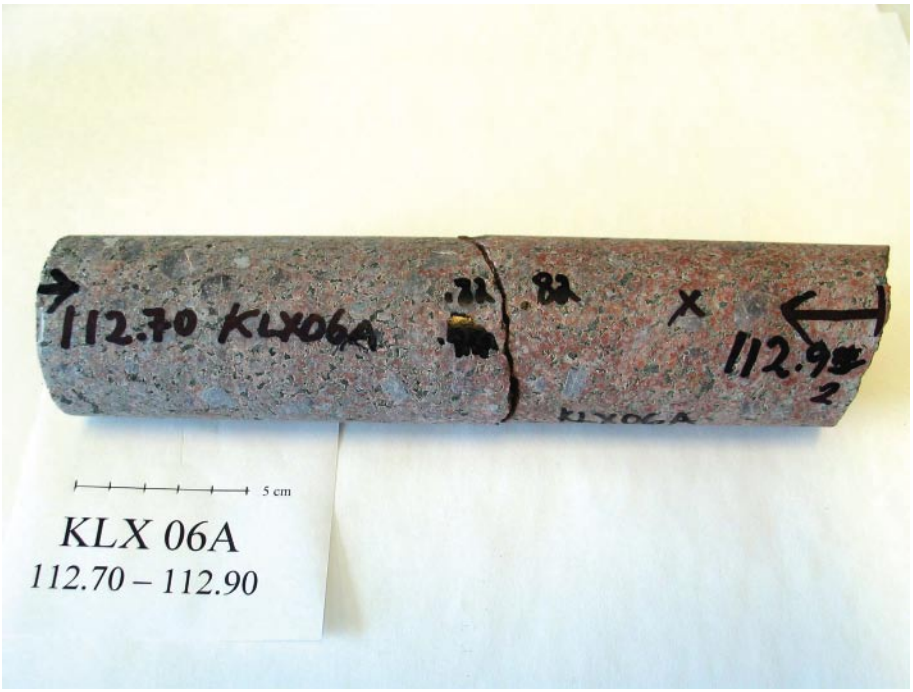

Figure A5-1. *The whole sample before analysis.*

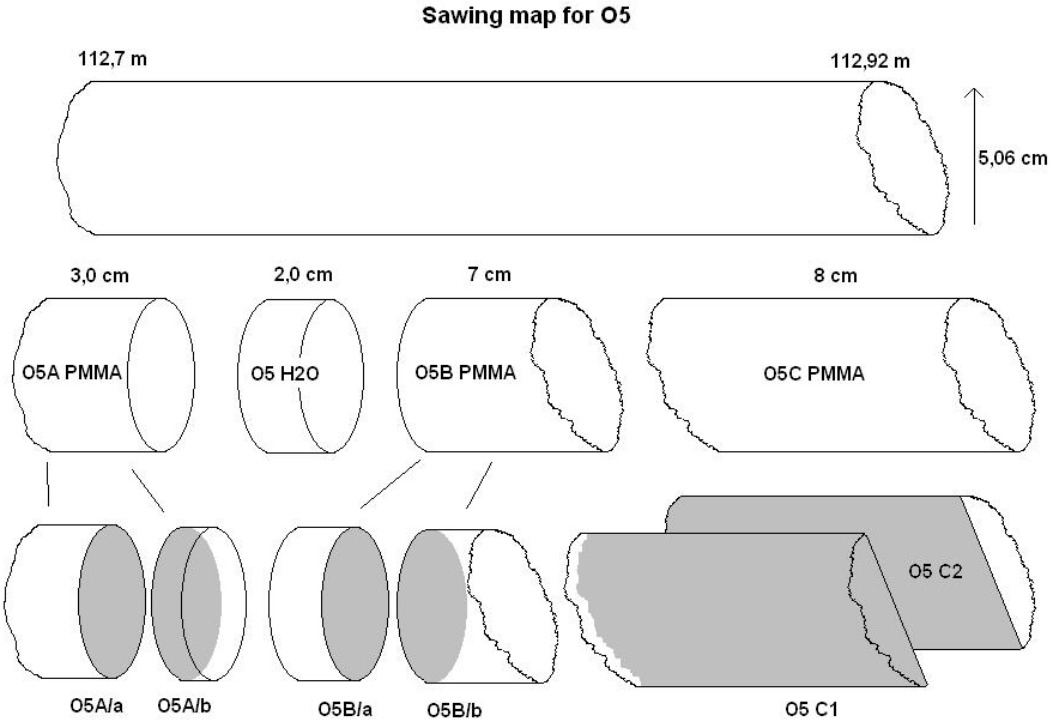

Figure A5-2. *Partition diagram for sample O5.*

Appendix 6

Worksheet for sample O6 (KLX06)

The photo images of sample O6 before any operation and the partition map for PMMA analyses and autoradiography. Shaded surfaces are autoradiographed.

Figure A6-1. *The whole sample before analysis.*

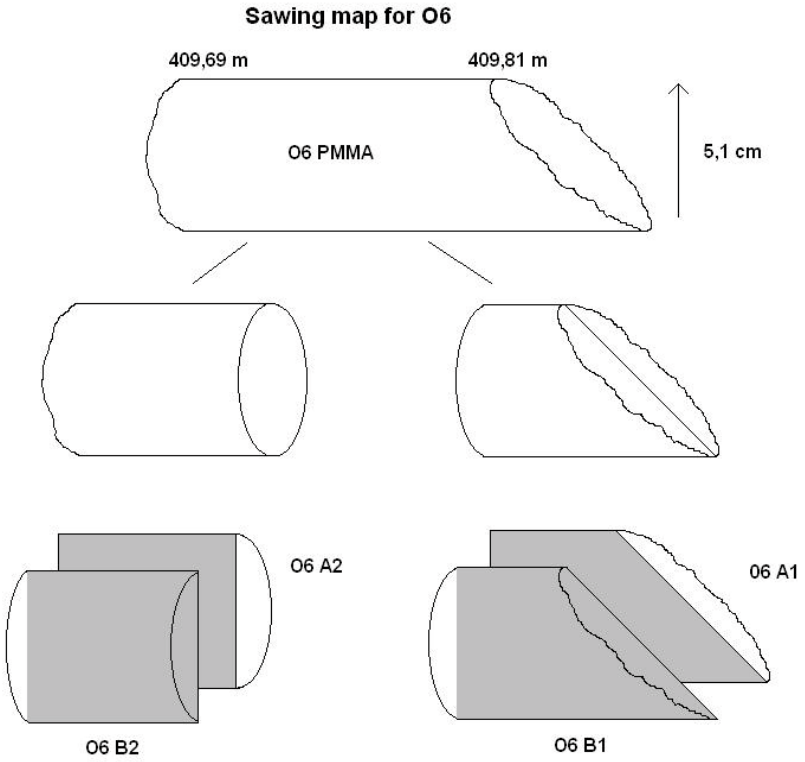

Figure A6-2. *Partition diagram for sample O6.*

Appendix 7

Worksheet for sample O7 (KSH02)

The photo images of sample O7 before any operation and the partition map for PMMA analyses and autoradiography. Shaded surfaces are autoradiographed.

Figure A7-1. *The whole sample before analysis.*

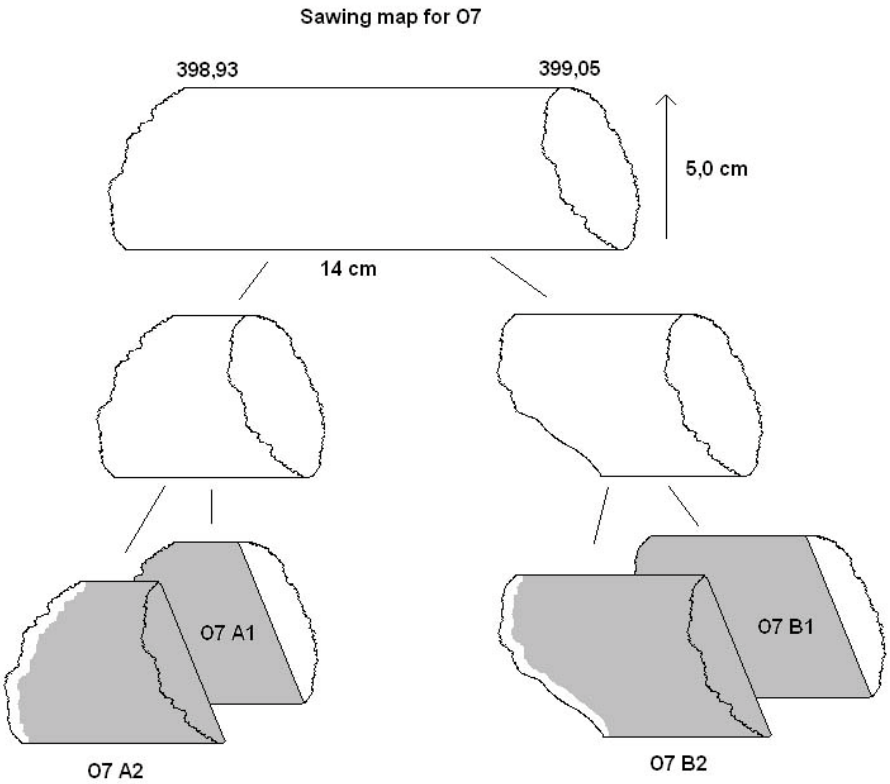

Figure A7-2. *Partition diagram for sample O7.*

Appendix 8

Worksheet for sample O8 (KSH02)

The photo images of sample O8 before any operation and the partition map for PMMA analyses and autoradiography. Shaded surfaces are autoradiographed.

Figure A8-1. *The whole sample before analysis. Lengths were later adjusted and correct lengths are given in Figure A8-2.*

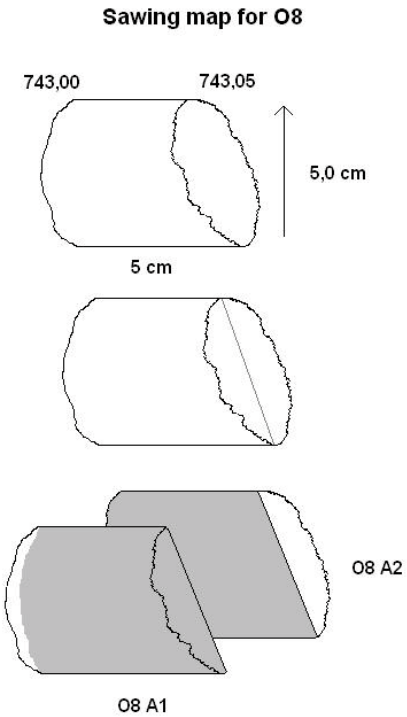

Figure A8-2. *Partition diagram for sample O8.*

Appendix 9

Worksheet for sample O9 (KLX02)

The photo images of sample O9 before any operation and the partition map for PMMA analyses and autoradiography. Shaded surfaces are autoradiographed.

Figure A9-1. *The whole sample before analysis.*

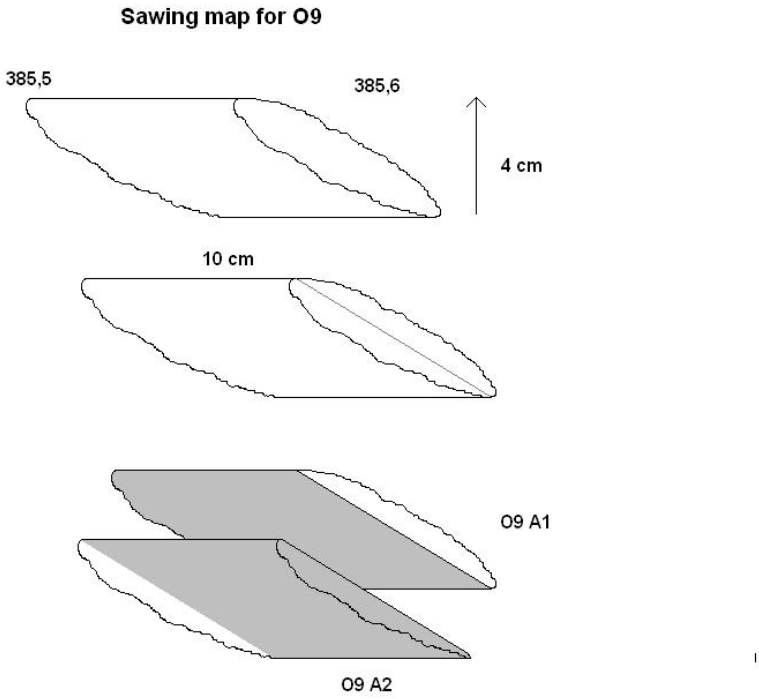

Figure A9-2. *Partition diagram for sample O9.*

Appendix 10

Worksheet for sample O10 (KLX03)

The photo images of sample O10 before any operation and the partition map for PMMA analyses and autoradiography. Shaded surfaces are autoradiographed.

Figure A10-1. *The whole sample before analysis.*

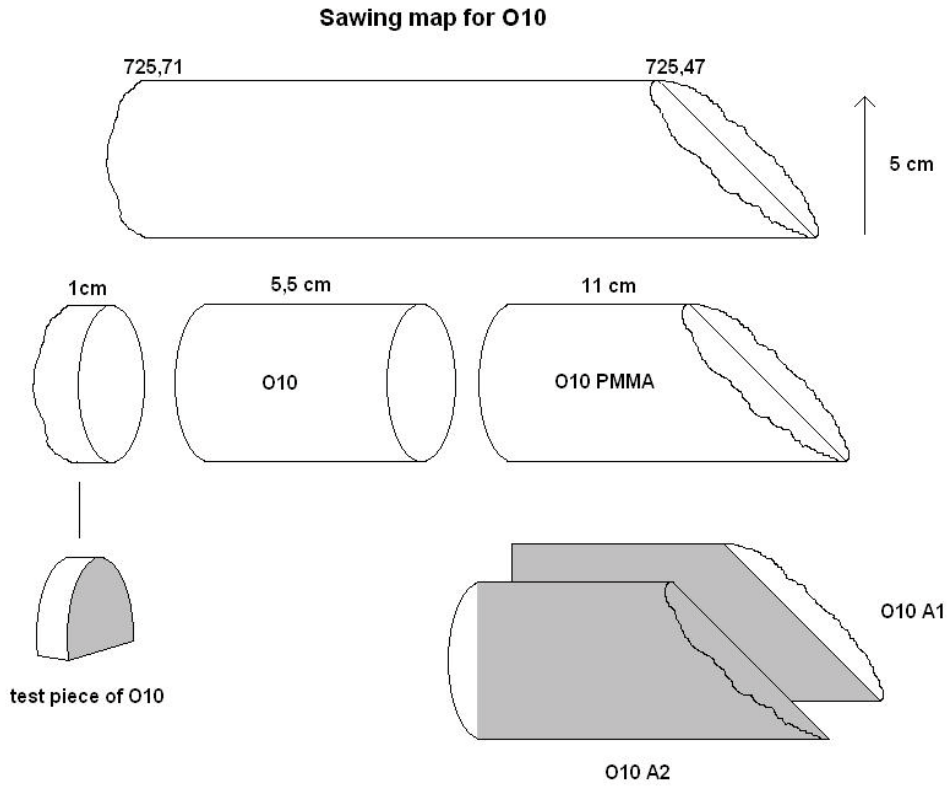

Figure A10-2. *Partition diagram for sample O10.*

Appendix 11

Worksheet for sample O11 (KLX04)

The photo images of sample O11 before any operation and the partition map for PMMA analyses and autoradiography. Shaded surfaces are autoradiographed.

Figure A11-1. *The whole sample before analysis.*

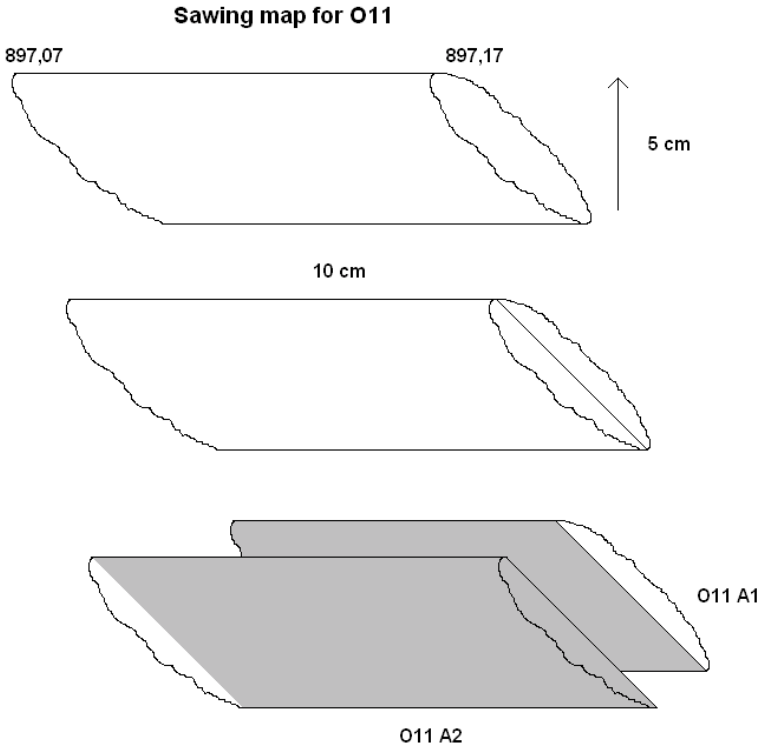

Figure A11-2. *Partition diagram for sample O11.*

Appendix 12

Worksheet for sample O12 (KLX04)

The photo images of sample O12 before any operation and the partition map for PMMA analyses and autoradiography. Shaded surfaces are autoradiographed.

Figure A12-1. *The whole sample before analysis.*

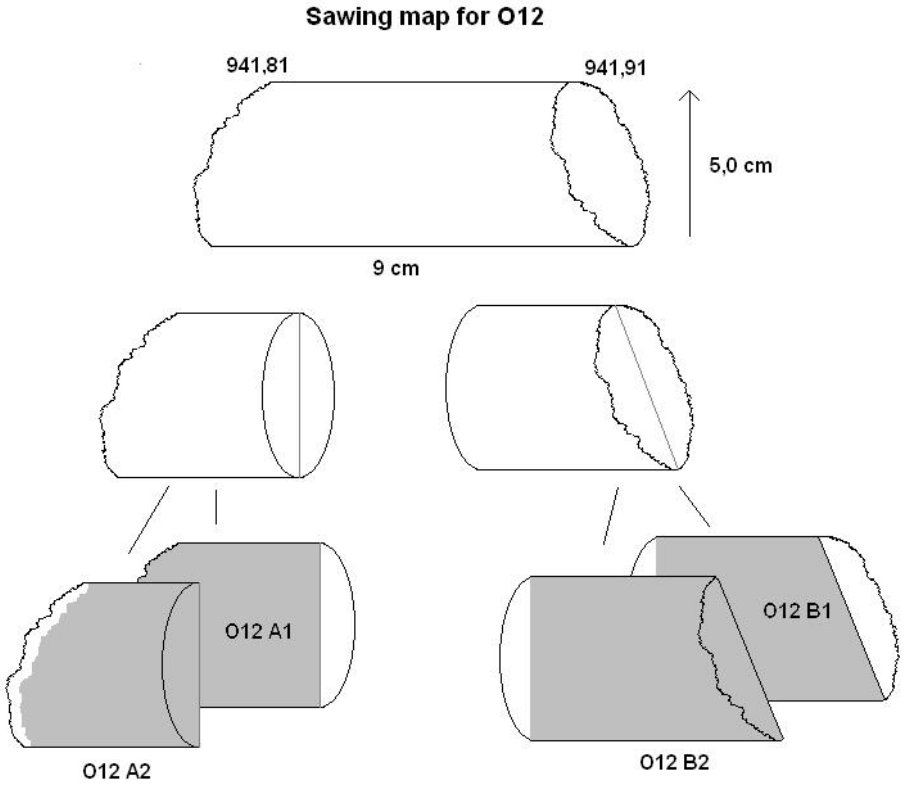

Figure A12-2. *Partition diagram for sample O12.*

Appendix 13

Worksheet for sample O13 (KLX05)

The photo images of sample O13 before any operation and the partition map for PMMA analyses and autoradiography. Shaded surfaces are autoradiographed.

Figure A13-1. *The whole sample before analysis.*

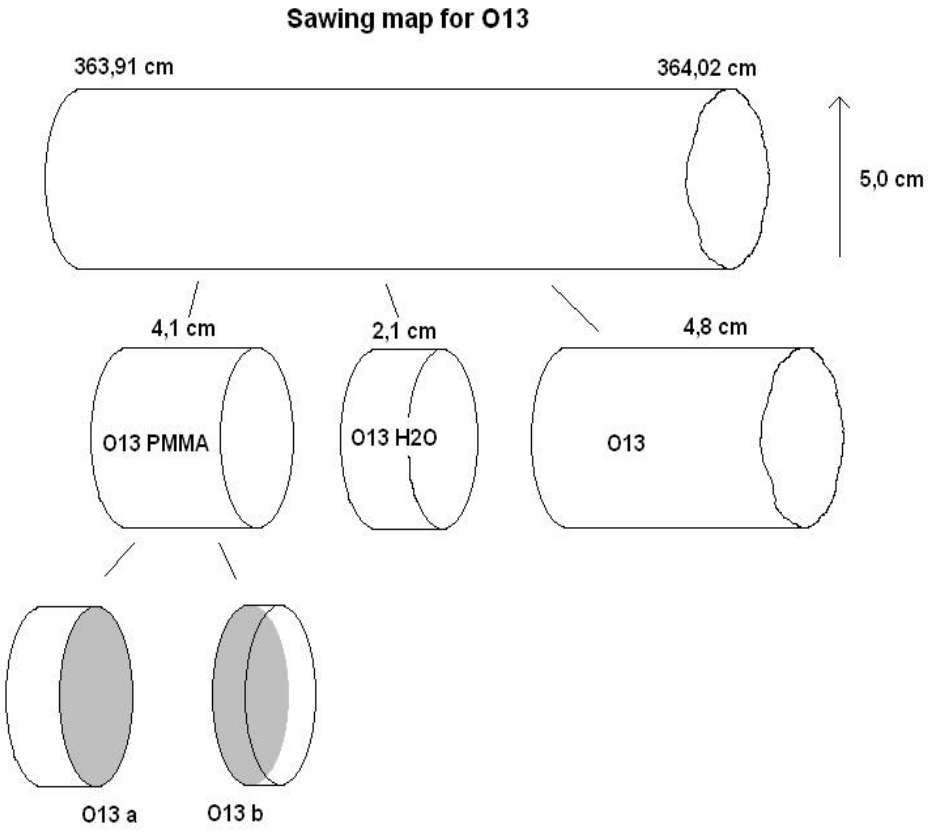

Figure A13-2. *Partition diagram for sample O13.*

Appendix 14

Worksheet for sample O14 (KLX05)

The photo images of sample O14 before any operation and the partition map for PMMA analyses and autoradiography. Shaded surfaces are autoradiographed.

Figure A14-1. *The whole sample before analysis.*

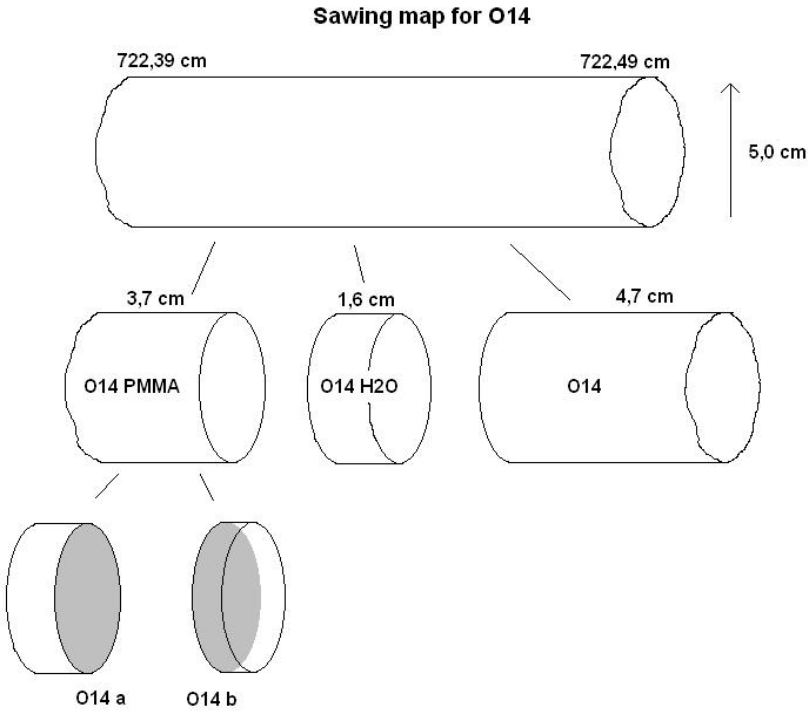

Figure A14-2. *Partition diagram for sample O14.*

Appendix 15

Worksheet for sample O15 (KLX06)

The photo images of sample O15 before any operation and the partition map for PMMA analyses and autoradiography. Shaded surfaces are autoradiographed.

Figure A15-1. *The whole sample before analysis.*

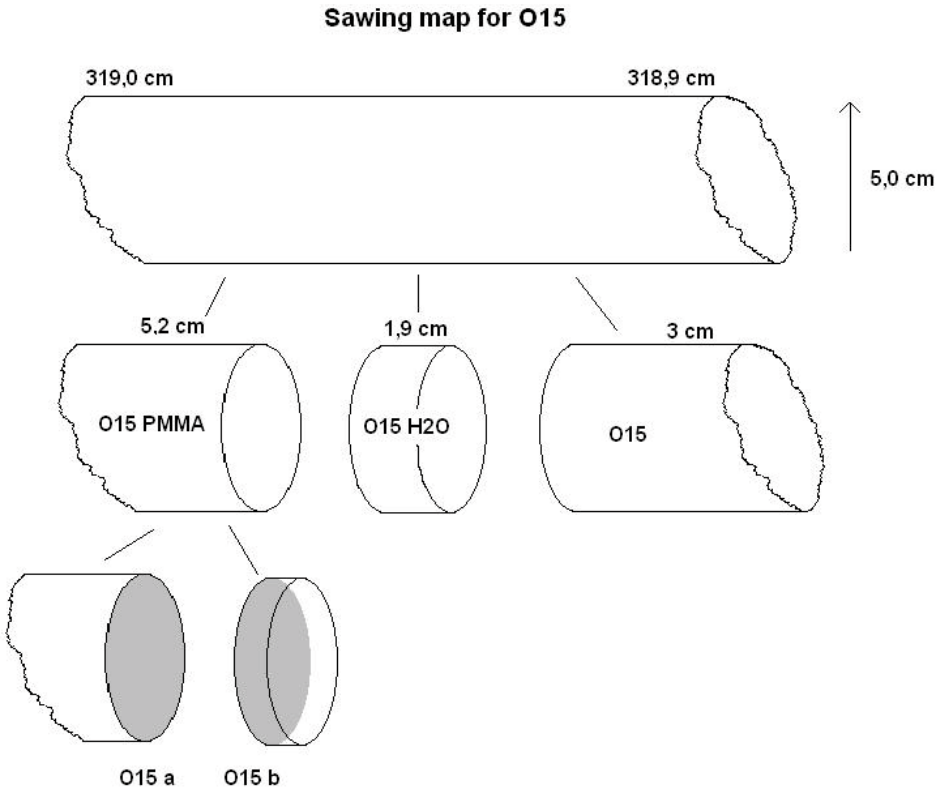

Figure A15-2. *Partition diagram for sample O15.*

Appendix 16

Worksheet for sample O16 (KSH02)

The photo images of sample O16 before any operation and the partition map for PMMA analyses and autoradiography. Shaded surfaces are autoradiographed.

Figure A16-1. *The whole sample before analysis.*

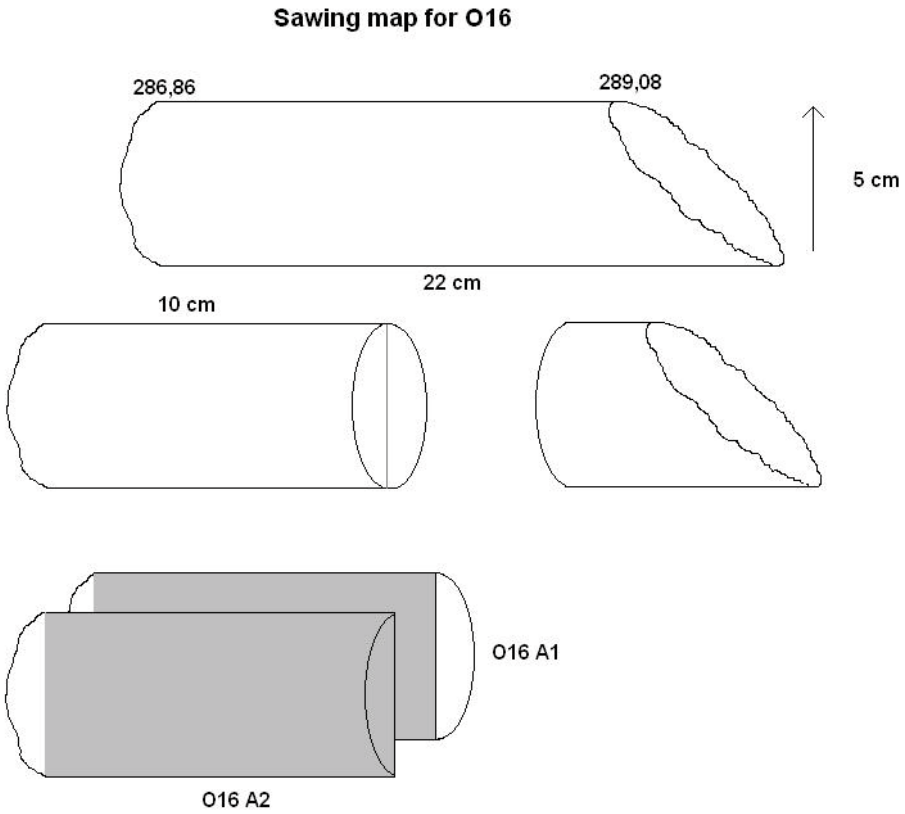

Figure A16-2. *Partition diagram for sample O16.*

Appendix 17

The initial data given by SKB

A short description of sample types and the adjusted depths (which could differ from the depths given in Appendix 1-16) of samples in the borehole are given.

HYRL code	Borehole	Secup	Seclow	Rock type	comments
O1	KSH01	714.89	715.04	Quartz monzonite to monzodiorite, equigranular to weakly porphyritic	
O2	KSH02	600.31	600.41	Granite, fine- to medium-grained	Medium alteration
O3	KLX02	216.56	216.66	Granite to quartz monzodiorite, generally porphyritic	
O4	KLX02	683.43	683.53	Fine-grained dioritoid (Metavolcanite, volcanite)	
O5	KLX06	112.70	112.92	Granite to quartz monzodiorite, generally porphyritic	Unaltered to medium altered wall rock close to open fracture
O6	KLX06	409.69	409.83	Granite to quartz monzodiorite, generally porphyritic	Open fracture with coating
O7	KSH02	398.93	399.05	Fine-grained dioritoid (Metavolcanite, volcanite)	“Zone” with fractures, mylonite and cataclasite
O8	KSH02	743.00	743.05	Fine-grained dioritoid (Metavolcanite, volcanite)	“Zone” with gouge and breccia fragments
O9	KLX02	385.50	385.60	Mafic rock, fine-grained	Altered rock with chlorite and clay minerals
O10	KLX03	725.47	725.72	Quartz monzonite to monzodiorite, equigranular to weakly porphyritic	Rock with network of partly opened and sealed fractures
O11	KLX04	897.07	897.17	Granite to quartz monzodiorite, generally porphyritic	Fracture with altered wallrock
O12	KLX04	941.81	941.91	Granite to quartz monzodiorite, generally porphyritic	Hydrothermal alteration
O13	KLX05	363.91	364.02	Diorite to gabbro	
O14	KLX05	722.39	722.49	Granite, fine- to medium-grained	
O15	KLX06	318.90	319.00	Granite, medium- to coarse-grained	
O16	KSH02	288.86	289.08	Fine-grained dioritoid (Metavolcanite, volcanite)	Fracture with slightly altered bedrock

Appendix 18

The experimental procedure for the studied Oskarshamn samples

HYRL code	SKB code	Length (mm)	Diameter (mm)	Drying time (d)	Drying temp (°C)	Tracer activity (kBq/ml)	Impregnation (d)	Radiation dose (kGy)	Exposure time (d)
O1	KSH01	28	50	9	95 ± 5	~ 520	25	75	21d
O2	KSH02	34	50	9	95 ± 5	~ 520	25	75	21d
O3	KLX02	34	47	9	95 ± 5	~ 520	25	75	21d
O4	KLX02	20	47	9	95 ± 5	~ 520	25	75	28d
O5A	KLX06	30	50	25	95 ± 5	~ 520	31	69	21d
O5B		70		7	100 ± 5	~ 560	19	68	21d
O5C		80		7	100 ± 5	~ 560	19	68	21d
O6	KLX06	130	51	4	92 ± 5	~ 520	22	77	7d, 21d
O7	KSH02	110	50	7	88 ± 5	~ 560	9	68	21d, 4d
O8	KSH02	46	50	9	46 ± 5	~ 75	14	102	6d
O9	KLX02	100	40	9	45 ± 5	~ 75	14	102	6d
O10	KLX03	10	50	3	85 ± 5	~ 40	22	68	21d
		110		17	74 ± 5	~ 190	29	95	8d
O11	KLX04	100	50	7	85 ± 5	~ 1,100	21	95	14d
O12	KLX04	85	50	7	57 ± 5	~ 40	21	95	7d
O13	KLX05	41	50	19	98 ± 5	~ 260	30	81	20d
O14	KLX05	37	50	11	88 ± 5	~ 220	19	81	20d
O15	KLX06	47	50	19	98 ± 5	~ 260	30	81	15d
O16	KSH02	117	50	17	92 ± 5	~ 190	29	95	25d